

**FINITE ELEMENT MODELLING OF A GMRT
ANTENNA**

**Submitted in Partial Fulfilment of the Requirements for the Degree
of**

Bachelor of Technology in

Aerospace Engineering

by

Bishwajit Gogoi

SC08B066

And

Karapurath Abhishekaran

SC08B076

Department of Aerospace Engineering

Indian Institute of Space Science and Technology

Thiruvananthapuram

April 2012

BONAFIDE CERTIFICATE

This is to certify that this project entitled “**FINITE ELEMENT ANALYSIS OF A GMRT ANTENNA**” submitted to **Indian Institute of Space Science and Technology, Thiruvananthapuram**, is a bonafide record of work done by “**BISHWAJIT GOGOI**” and “**KARAPURATH ABHISHEKARAN**” under my supervision from “**9th January 2012**” to “**26th April 2012**”.

<<Signature of the Supervisor>>

<<Name and designation>>

<<Signature of the Supervisor>>

<<Name and designation>>

<<Countersignature>>

<<Name>>

<<Designation>>

<<Name of dept, division and centre>>

Place:

Date:

Declaration by Authors

This is to declare that this report has been written by us. No part of this report is plagiarized from other sources. All information included from other sources has been duly acknowledged. We aver that if any part of the report is found to be plagiarized, we shall take full responsibility for it.

Bishwajit Gogoi

SC08B066

Karapurath Abhishekarani

SC08B076

Place:

Date:

Abstract

Table of Contents

Chapter 1 INTRODUCTION

1.1	Background scenario	7
1.2	Scope.....	7
2.1	Software Packages	9
2.1.1	STAAD-Pro	9
2.1.2	ANSYS	9
2.2	Modelling of the dish structure:	9
2.2.1	Assumptions.....	9
2.2.2	Staad methodology.....	9
2.2.2.1	Model creation.....	10
2.2.2.2	Applicable loads	12
2.2.2.3	Permissible stresses	14
2.2.2.4	Material property.....	14
2.2.2.5	Stress ratio	14
2.2.3	Ansys methodology	15
2.2.3.1	Modeling Methodology:.....	15
2.2.3.2	Antenna modelling:.....	17
2.2.3.3	Loading.....	17
2.2.4	Wind loads	17
2.2.4.1	Reduction Factor (K):.....	17
2.2.4.2	Drag Force on members:	18
2.2.4.3	Coefficient of Drag:.....	18
2.2.4.4	Design wind speed:.....	18
2.2.4.5	Risk Coefficient:.....	18
2.2.4.6	Terrain roughness and size factor:.....	19
2.2.4.7	Topography Factor:	20
2.2.5	Calculation of Wind loads on structure:	20
2.2.6	Wind loads on mesh:.....	21
2.2.7	CFD:.....	23
2.2.8	CORROSION:	27
2.2.8.1	Model Information:.....	27
2.2.8.2	Modelling Methodology:.....	28

Chapter 3 RESULTS AND DISCUSSIONS

3.1	ANSYS WORKBENCH RESULTS	31
3.1.1	Cylindrical wire:	31
3.1.2	CFD on Wire Mesh:.....	32
3.2	STAADPRO V8i RESULTS	37
3.2.1	Finite element model.....	37
3.2.1.1	Coordinate system	38

3.2.1.2 Rope truss system	38
3.2.1.3 Cross bracing system	38
3.2.1.4 Boundary conditions	38
3.2.2 Dead load case	39
3.2.2.1 Configuration:	39
3.2.2.2 Maximum stress ratio reached for Feed load = 1300 kg	39
3.2.2.3 Deflection of feed under different orientation for feed load =1300 kg	40
3.2.2.4 Inference	40
3.2.3 Wind load case	40
3.2.3.1 TCE vs. TWL	40
3.2.3.2 Operating wind speed	41
3.2.3.3 Analysis for Maximum wind speed in Nashik region 140 kmph	41
3.2.3.4 Analysis for survival wind speed.....	41
3.2.4 Ansys Mechanical vs. Staad.Pro V8i	41
3.2.4.1 Configuration.....	41
3.3 ANSYS MECHANICAL RESULTS	43
3.3.1 Inference	47
3.4 ANSYS CORROSION RESULTS:	49
3.4.1 Inference	54

1. Introduction

1.1 Background scenario

The National Centre of Radio Astrophysics (NCRA) of Tata Institute of Fundamental Research (TIFR), Pune has set-up a unique facility for radio astronomical research using the meter wave range of the radio spectrum, known as Giant Meter-wave Radio Telescope (GMRT) at Khodad. GMRT consists of 30 parabolic dishes of 45 m in diameter arranged in a Y pattern.

GMRT (Giant Metre wave Radio Telescope) is a world renowned radio astronomical facility which attracts nearly 70% of its users from abroad. In the last 16 years it has been operational; it has survived many a nature's wrath. Such a long exposure to atmosphere has led to corrosion at a few members of antennas. This in turn has led to a reduction in the load taking ability of the antenna structure. Since the structure was highly optimised initially and has a very few redundant members, the reduction in load taking ability may affect the shape of the parabolic face of the antenna and render it unusable for astronomical data collection.

1.2 Scope

This project deals with the finite element modelling of the GMRT antenna in STAAD-Pro and ANSYS 13.0 and the analysis of stresses and strains at different locations of the antenna for different load conditions. It also deals with the incorporation of corrosion into the FE model and its subsequent consequences.

The data obtained in this project will be utilised in the maintenance of the antennas. Assessment of the stresses would help in the better understanding of the antenna structure. An in-house code will be built in the process which will act as a platform for any future simulations. An inspection of the antennas has led to the realisation that a few members of certain antennas have incurred heavy corrosion damage. A preferential order for their replacement has to be made. A proper approximation of the reduction in load taking abilities of such members will serve as a guiding light for such replacements.

Such a similar project was undertaken by Tata consulting engineers limited. Their report on "Structural analysis of GMRT antenna using STAAD-Pro package" has addressed some of

the concerns dealt with in this report. The report by TCE has been used as a guiding light for this project.

The stresses at different locations have been modelled and analysed. A Computational fluid dynamics simulation was conducted to check for the drag on the wire mesh. An approximation for the corrosion was applied and its effects on the integrity of the structure has been analysed.

2. Methodology

2.1 Software Packages

2.1.1 STAAD-Pro

STAAD Pro is a general purpose structural analysis and design program with applications focusing primarily on the building industry. Commercial buildings, bridges and highway structures, industrial structures, chemical plant structures, dams, retaining walls, turbine foundations, culverts and other embedded structures can be modelled with ease in STAAD. It has inbuilt design codes, material data, common cross sections etc. which help in easy and fast analysis of a common structure. This also limits the functionality of the software as the incorporation of custom sections in STAAD is very complex. STAAD is not very accurate in analysing very small structures, finding concentrated stresses, damage analysis etc.

2.1.2 ANSYS

ANSYS is a very powerful package whose capabilities are practically limitless. ANSYS Mechanical APDL which is the FEM package in ANSYS is not as simple as STAAD but can be used to model structures both small and large with superior accuracy. It has a complex GUI which is hard to use. ANSYS offers flexibility in modelling at the cost of simplicity.

2.2 Modelling of the dish structure:

2.2.1 Assumptions

Before we started the modelling there are a few assumptions me made. Instead of doing a full FEM analysis of the entire antenna structure we have selected only the dish along with the quadripod and the feed system for the analysis. Our argument is that the yoke structure and the concrete pillar support are structurally much stronger than the dish and thus any form of structural failure will happen at dish first.

2.2.2 Staad methodology

STAAD.Pro is a general purpose program for performing the analysis and design of a wide variety of types of structures. The basic three activities which are to be carried out to achieve that goal –

- a) model generation
- b) the calculations to obtain the analytical results
- c) result verification - are all facilitated by tools contained in the program's graphical environment

One can create a model using either

- Using the graphical model generation mode
- The command file mode using Staad editor.

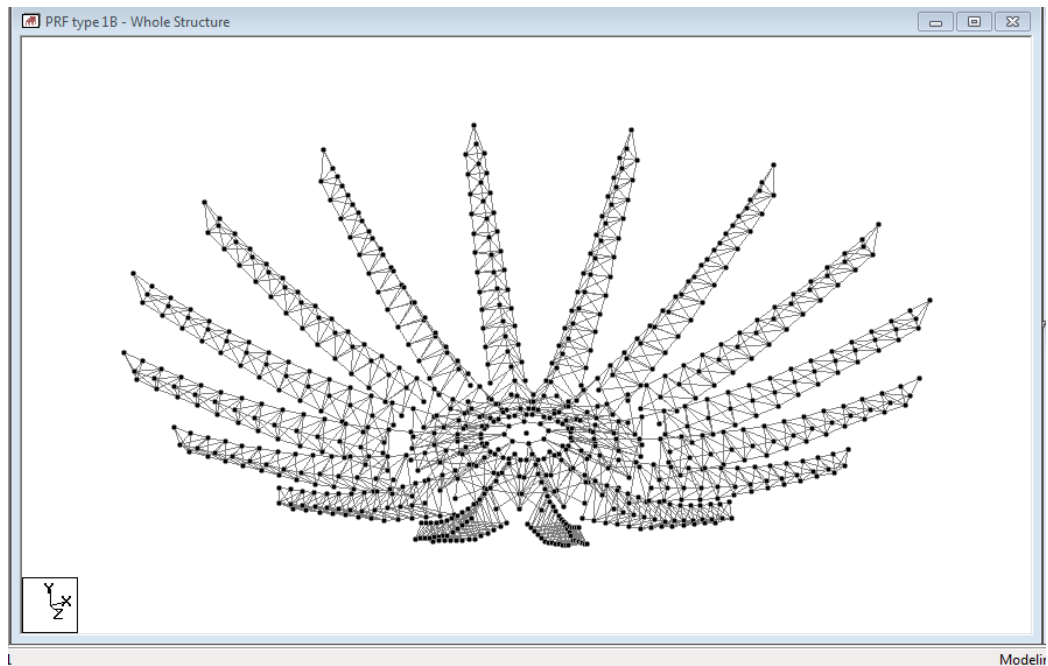
The graphical model generation mode and the command file are seamlessly integrated. So, at any time, you may temporarily exit the graphical model generation mode and access the command file. In our modelling we have preferred using the command file mode as it is easier to handle the large number of nodes and beams used.

The following demonstrates the basic algorithm one can use to create and define a model

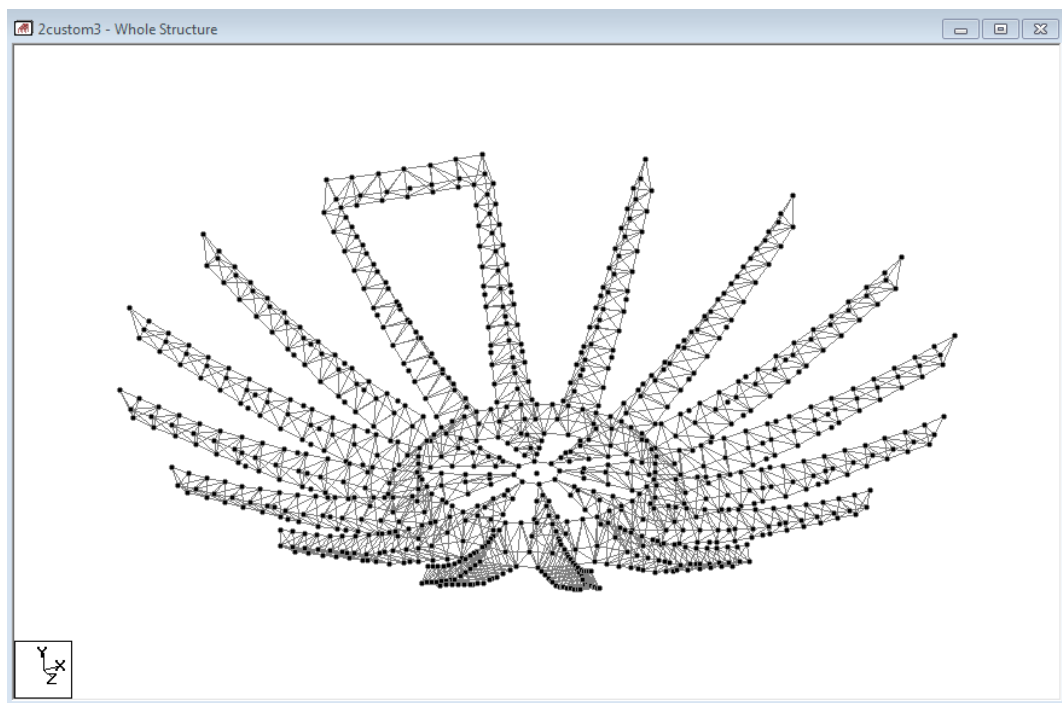
1. Define the node points.
2. Join the node points.
3. Define the cross-sections and material properties of the members.
4. Define the supports.
5. Define the load cases and assign them to the respective members.
6. Define the type of analysis to be performed.
7. Choose the required building code for code check
8. Perform analysis
9. The post processing is GUI based. One can also use SQL database to snatch specific values from the analyzed lot.

2.2.2.1 Model creation

- We used a systematic step by step approach to create the model. We first started with the PRFs first. A single PRF, the one aligned along the positive X-axis was created from the coordinates calculated using MS Excel. The PRF was copied and rotated every 22.5 degrees. So we now have a 16 PRF structure.
 - Pipe cross-sections were added and assigned to all the beams.

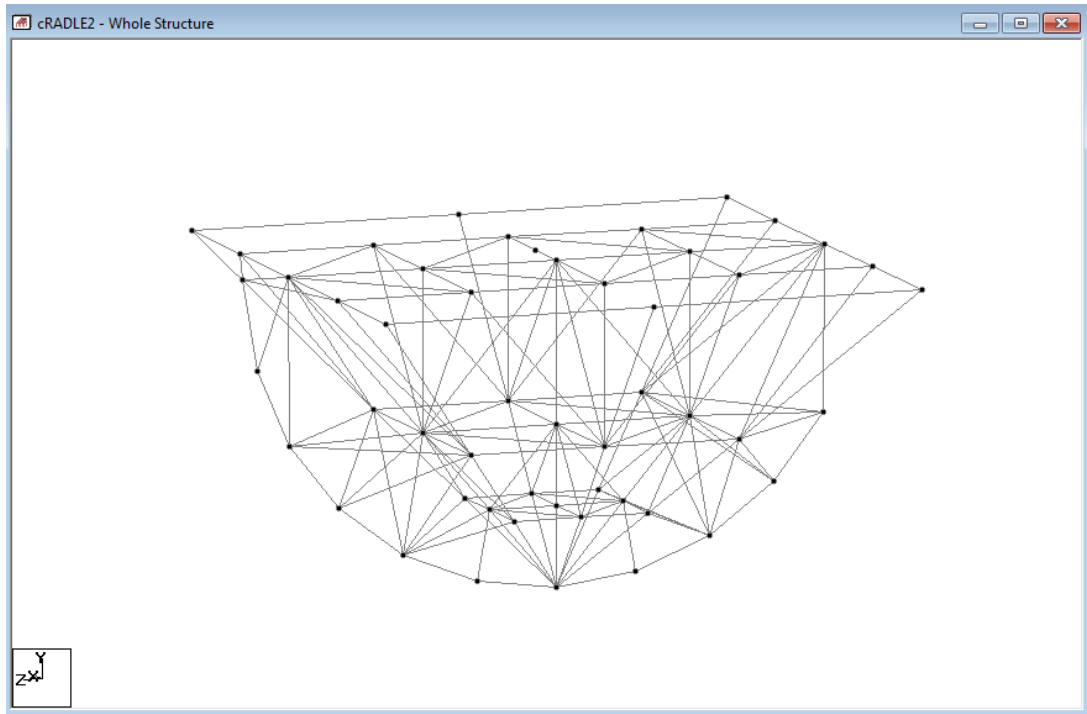


- Then we used Autocad 2011 to design the rim structure around the PRF skeleton structure. It would have been a more tedious exercise if we had to fall back to the MS Excel sheet as the Rim has an overall curved structure.
 - All the pipe cross-sections were added to the Rim and then rotated.



- The Hub and its three faces were created in situ around the PRF structure.
 - All the pipe cross-sections were added to the Hub and then rotated.

- The Cradle was finally created as a separate structure and then its origin was shifted to finally integrate it into the final structure.
 - All the pipe cross-sections were added to the Cradle.



2.2.2.2 *Applicable loads*

2.2.2.2.1 *Dead Loads*

Dead load includes the self-weight of the structural members, reflector mesh, turnbuckle, etc. And an extra 10% is considered to take into account weights of the connections, access ladders, and maintenance platform. Etc.

2.2.2.2.2 *Wind loads*

The wind loads were applied on mesh and the members for different wind speeds.

When we first started with our calculation of the wind loads, we had two choices.

1. The TCE methodology. In this method TCE calculated the wind loads by always considering the wind vector perpendicular to each member axis. This is a larger approximation, as wind load is calculated along for the entire length.
2. We devised a method in which we can actually calculate the wind loads on the projected member length. This methodology is explained in more exhaustive detail under WIND LOADS section.

2.2.2.2.3 Other Loads

A pay load of 1300 kg (weight of the total feed, support structure and it's drive system) is considered in the analysis.

2.2.2.2.4 Load combinations

In the present analysis 12 primary load cases are considered as described in the **Table** below. Erection load is not considered in the load combination,

The primary loads and their load combinations which are used in STAAD-PRO solving process are as follows.

S.NO	LOAD	NOTATION
1	Feed load	L1
2	Dead load	L2
3	Counter-Weight	L3
4	Pretension	L4
5	TCE wind load +X WG NS members	L5
6	TCE wind load +Z WG NS members	L6
7	TCE wind load +X NG NS mesh	L7
8	TCE wind load +Z NG NS mesh	L8
9	TWL wind load +X WG NS members	L9
10	TWL wind load +Z WG NS members	L10
11	TWL wind load +X NG NS mesh	L11
12	TWL wind load +Z NG NS mesh	L12

Also, we had two choices when we had to apply the loads in tandem.

- Load combination: A load combination is a set of load results which are combined algebraically to produce a superimposed set of results for post-processing. Therefore, a load combination instructs the program to take the results of previously solved primary load cases, factor them appropriately, and combine the values using ALGEBRAIC, SRSS or ABSolute methods.
- Repeat load: A Repeat Load type looks remarkably like a load combination type, but is in fact a primary load type. It differs from a load combination type in that the program actually analyses the structure (that is, it solves the matrix equation $[K]\{d\} = \{P\}$) for a repeat load case, where as it merely adds up the results for a combination case. We have to use Repeat Load types to obtain results of one or more load cases acting in tandem.

As our model doesn't have any major nonlinear elements except the cross bracings which are 'tension only members' the combination load option is adequate. We still tried both methods

and found out that combination loads give smaller deflection values compared to repeat loads.

S. NO	LOAD	COMBINATION
1	TCE Wind in +X direction	L1+ L2 + L3 + L4 + L5 +L7
2	TCE Wind in -X direction	L1+ L2 + L3 + L4 - L5 - L7
3	TCE Wind in +Z direction	L1+ L2 + L3 + L4 + L6 + L8
4	TCE Wind in -Z direction	L1+ L2 + L3 + L4 - L6 - L8
5	TWL Wind in +X direction	L1+ L2 + L3 + L4 + L9 +L11
6	TWL Wind in -X direction	L1+ L2 + L3 + L4 - L9 - L11
7	TWL Wind in +Z direction	L1+ L2 + L3 + L4 + L10 + L12
8	TWL Wind in -Z direction	L1+ L2 + L3 + L4 - L10 - L12

2.2.2.3 Permissible stresses

Permissible stresses in the structure are as per IS 800-1984 and are indicated in [Table- below](#).

Sr. No.	Nature of Stress	Normal permissible Stress	Para in IS 800	Permissible stress for survival wind speed loading
1	Axial Tension	0.6*fy	4.1.1	0.8*fy
2	Axial Compression	0.66*fy	5.1.1	0.88*fy
3	Bending	0.66*fy	6.2.1	0.88*fy
4	Equivalent	0.9*fy	7.1.4	0.9*fy

2.2.2.4 Material property

All structural tubes are of Yst-210 quality steel (as per IS-1161-1979) having yield strength of 215 Mpa. Rope truss is of stainless steel AISI-304 quality having yield strength of 205 Mpa (as per IS-1161-1979). (Reference is made to IS: 1161-1979 as the original design calculations comply to it and not to the latest revision in IS:1161-1998).

2.2.2.5 Stress ratio

Stress Ratio is ratio of the actual to allowable stresses. Stress ratio is the combination of stress induced in the member due to axial tension or compression and bending in other direction. Stress Ratio should be less than or equal to 1.0. as indicated below

a) Combined axial compression and bending

$$\frac{\sigma_{ac, cal}}{\sigma_{ac}} + \frac{\sigma_{bcx, cal}}{\sigma_{bcx}} + \frac{\sigma_{bcy, cal}}{\sigma_{bcy}} \leq 1.0$$

b) Combined axial tension and bending

$$\frac{\sigma_{at, cal}}{\sigma_{at}} + \frac{\sigma_{btx, cal}}{\sigma_{btx}} + \frac{\sigma_{bty, cal}}{\sigma_{bty}} \leq 1.0$$

σ_{at} , cal	Stress in Axial tension
σ_{ac} , cal	Stress in Axial Compression
σ_{bc} , cal	Stress in bending compression in y and x direction
σ_{bt} , cal	Stress in bending tension in y and x direction
σ_{ac}	0.6 fy, Permissible Axial Stress
σ_{bt}	0.66 fy, Permissible Bending Stress

2.2.3 Ansys methodology

ANSYS is a very powerful package whose capabilities are practically limitless. ANSYS Mechanical APDL which is a Finite element package in ANSYS is not as simple as STAAD but can be used to model structures both small and large with superior accuracy. It has a complex GUI which is hard to use. It offers both flexibility and accuracy in modelling at the cost of simplicity.

2.2.3.1 Modeling Methodology:

One of the most important aspects of modelling in ANSYS is the proper selection of appropriate elements. ANSYS offers many elements for modelling and each element has its pros and cons.

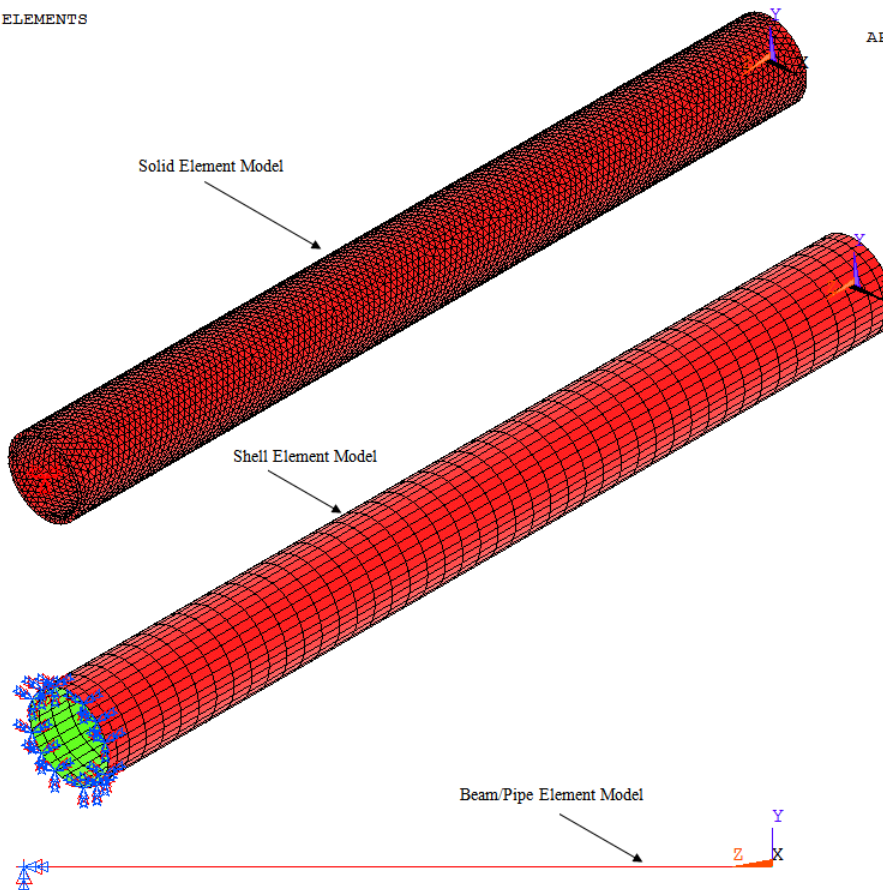


Figure 1: The visual difference in using different elements

To explore the possibility of the usage of different elements to model the GMRT antenna, we selected 4 elements; PIPE288, BEAM188, SOLID285 and SHELL181 based on their compatibility for modelling cylindrical structures. These elements were checked for their accuracy, ease of modelling large structures and the required computational power by modelling a simple cylindrical beam subjected to a tensile load at one end and fixed at the other. Figure 1 depicts the visual difference in the models. It can be noticed from Figure 1 that the beam/pipe element model seems very simple. It can only be used when the structure has a piecewise constant cross section. Shell elements on the other hand can only be used where there is a piece wise constant thickness. Solid elements can model any structure.

It was noticed from the modelling that all the elements gave nearly the same result for displacement and stresses. But modelling the cylindrical pipe using PIPE288 took the least time and was the simplest in modelling. Hence, PIPE288 was used to model the members of the antenna.

2.2.3.2 Antenna modelling:

The ANSYS model was created by mostly utilizing the command prompt. The keypoints obtained previously were input to excel and the respective commands were created using the concatenate feature in excel. These commands were input to the pre-processor in ANSYS.

The keypoints were joined by using the line between keypoints feature in the pre-processor of ANSYS to create the skeleton structure of the antenna. The material properties were input. The lines created were numbered in a way to provide easy identification. A database was created which associates the line number of the line in ANSYS to the diameter and thickness of the pipe that line represents. These sections were numbered for identification and were created using the same numbering by using the section feature in ANSYS. The concatenate feature of excel was used to generate the command to assign the particular section to the line and mesh it. The elements were sized using smart sizing.

2.2.3.3 Loading

The dead weight was added as a gravitational field in ANSYS. An extra 10% gravitational field was added to accommodate for the joints, screws, plates and other small structures which were ignored during the modelling. The weight of the feed was added at the cage support truss in the form of pressure on lines. The wind loads calculated in previously were added to the model. The two points on the cradle which are supported on the bearing were fixed for all degrees of freedom and a static analysis was conducted for different positions of the antenna.

The cross braces and the rope truss are pre-stressed members. This could not be modelled properly in ANSYS; hence the tension in these members has been added as a point load at the point where these pre-stressed members have been attached at the PRF.

2.2.4 Wind loads

The Indian standard code of practice for design loads for buildings and structures [1] has been used to estimate the wind loads on the members of the antenna structure. The 45m GMRT antenna is an unclad structural frame. The wind loads have been calculated as per Para 6.3.3.2 of [1].

2.2.4.1 Reduction Factor (K):

The Force coefficients given in [1] are for members of infinite length. These calculations have ignored the edge effects on the wake. To account for the edge effects a factor called “Reduction factor” is employed. Most of the members of GMRT antenna have a gusset plate

or a cross member at their ends. Due to these there would be no air flow near the edges, hence the Reduction factor has been assumed to be 1 at all places for the antenna.

2.2.4.2 Drag Force on members:

The model of the GMRT antenna has all cylindrical members, according to [1] the force on such members will be :

$$F = C_D * q * K * l_{eff} * D = C_D * \frac{1}{2} \rho V_Z^2 * K * l_{eff} * D \quad \{1\}$$

2.2.4.3 Coefficient of Drag:

The coefficient of drag for circular members is given in Table 1. The coefficient of drag is a function of Reynolds's number. Table -27 of [1] gives the values of coefficient of drag at different Reynolds's number for cylindrical members.


Plan Shape		$V_Z b \text{ m}^2/\text{s}$	C_f for Height / Breadth Ratio		
			≤ 2	10	≥ 20
	All Surfaces	< 6	0.7	0.9	1.2
	Rough or with projections	≥ 6			
	Smooth	≥ 6	0.5	0.5	0.6

Table 1: Table giving the values of force coefficient

Appropriate drag values were used as per Table 1.

2.2.4.4 Design wind speed:

The design wind speed acting on a structure is obtained by modifying the Basic wind speed by using factors K_1 , K_2 , K_3 according to [1]. The basic wind speed profile is obtained by averaging the peak gust velocity over a 3 second time interval. This doesn't include the effect of tornadoes. According to [1] the basic wind speed in Pune is 39m/s. The Design wind speed is given as :

$$V_Z = V_b * K_1 K_2 K_3$$

2.2.4.5 Risk Coefficient:

The risk coefficient or the probability factor " K_1 ", is a factor that accounts for the predicted life span of the structure and the degree of hazard they pose to life and property. Table 2 suggests the probable values of K_1 . As per GMRT's current configuration, a factor of 0.94 has been chosen.

Class of Structure	Mean Probable design life of structure in years	k_1 factor for Basic Wind Speed (m/s) of					
		33	39	44	47	50	55
All general buildings and structures	50	1.0	1.0	1.0	1.0	1.0	1.0
Temporary sheds, structures such as those used during construction operations (for example, formwork and false work), structures during construction stages, and boundary walls	5	0.82	0.76	0.73	0.71	0.70	0.67
Buildings and structures presenting a low degree of hazard to life and property in the event of failure, such as isolated towers in wooded areas, farm buildings other than residential buildings, etc.	25	0.94	0.92	0.91	0.90	0.90	0.89
Important buildings and structures such as hospitals, communication buildings, towers and power plant structures	100	1.05	1.06	1.07	1.07	1.08	1.08

Table 2: Values of Risk coefficient with wind speed for different design requirements

2.2.4.6 Terrain roughness and size factor:

The terrain roughness and size factor " K_2 " is a factor which accounts for the effects the terrain, the height and size of the structure have on the wind speeds. Table 3 suggests the values of K_2 . Appropriate values have been taken for the members considering their height from the ground. The terrain at Khodad is almost plain and the structure is taken to be under category 1.

Height (z) (m)	Terrain and height multiplier (k_2)			
	Terrain Category 1	Terrain Category 2	Terrain Category 3	Terrain Category 4
10	1.05	1.00	0.91	0.80
15	1.09	1.05	0.97	0.80
20	1.12	1.07	1.01	0.80
30	1.15	1.12	1.06	0.97
50	1.20	1.17	1.12	1.10
100	1.26	1.24	1.20	1.20
150	1.30	1.28	1.24	1.24
200	1.32	1.30	1.27	1.27
250	1.34	1.32	1.29	1.28
300	1.35	1.34	1.31	1.30
350	1.37	1.36	1.32	1.31
400	1.38	1.37	1.34	1.32
450	1.39	1.38	1.35	1.33
500	1.40	1.39	1.36	1.34

Table 3: Table giving the values of Terrain factor for different heights of structure

2.2.4.7 Topography Factor:

The topography factor accounts for the change in wind speeds caused by hills etc. Since the area around Khodad is fairly plain, K_3 is taken to be equal to 1.

2.2.5 Calculation of Wind loads on structure:

The wind load on the numerous members of the antenna would be very tedious to calculate for every member separately. Hence a vectorial method was used to calculate the direction and magnitude of wind loads on each member. Each beam of the structure was represented in vectorial form by using the nodes at their end points. The obtained beam vectors were projected onto a plane perpendicular to the unit incoming wind vector by taking a cross product to obtain the effective length. Figure 1 depicts graphically the interaction of wind vector with the beam vector. Here \vec{W} is the unit incoming wind vector and \vec{B} is the beam vector. The magnitude of the obtained vector is the effective length which is used to calculate the wind force on the member using formula {1}.

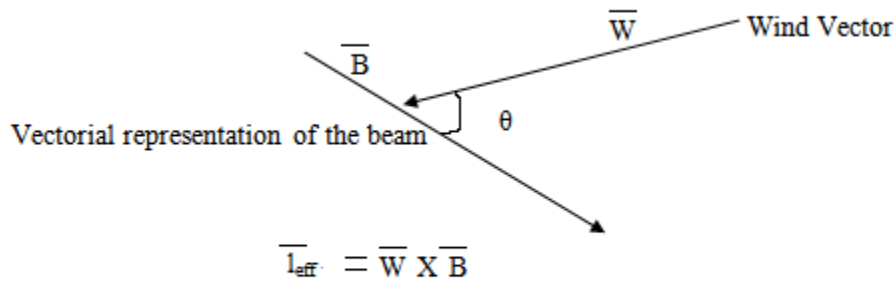


Figure 2: Interaction of beam vector and the incoming wind vector

An excel sheet was made to calculate the wind force on each member. Logical operators were used to assign values of K_1 , K_2 , and K_3 to each member. The Magnitude of Wind force obtained is multiplied with the unit wind vector to obtain the wind force vector.

2.2.6 Wind loads on mesh:

The wire mesh is the structure which is expected to give large wind loads. The coefficients of drag which exist for these types of meshes are crude approximate of the real phenomenon. CFD simulations were conducted to find values of force coefficients closer to reality. The force coefficients obtained from those simulations were incorporated to calculate the wind loads on mesh which were transferred to the top chord of the PRF.

Each chord of the PRF is separated by an angle of 22.5 degrees. If i and j are two consecutive nodes on the PRF, and if R_i and R_j are the radial distances to the nodes from the centre, Ao the shaded area in Figure 2. The force coefficients will change with the angle of attack, a dot product between incoming wind vector (\vec{W}) and the mesh normal vector (\vec{M}) is done to calculate the angle of attack. The force coefficients for this angle of attack are taken for wind load calculations for that portion of the mesh. The drag and the lift forces on the shaded portion can be calculated as shown in Figure 2.

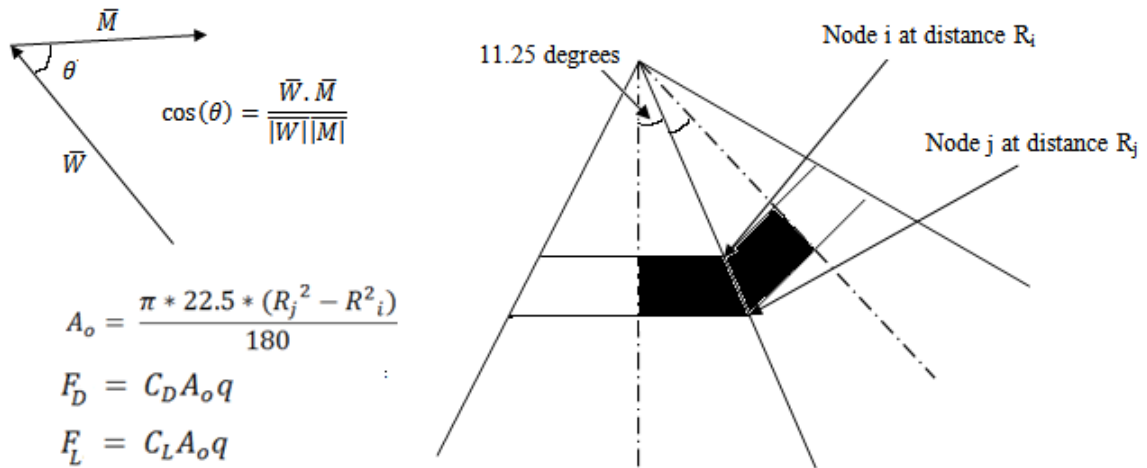


Figure 3: Method to calculate wind forces on mesh

The mesh loads were calculated for different portions of the mesh using MS Excel and substituted as point loads on the nodes of the top chord of the PRF.

References :

[1]-Indian standard code of practice for design loads (other than earthquakes) for buildings and structures, part -3: Wind loads, IS:875 (part-3) – 1987

2.2.7 CFD:

The parabolic reflecting surfaces on the GMRT antennas are made from low solidity wire meshes. This is because these antennas operate at wavelengths larger than 6cm and do not require a high solidity reflector. The wire meshes used in the GMRT antennas are made of cylindrical wires of diameter 0.55mm and sizes 10mm x 10mm, 15mm x15mm and 20mm x 20mm. The Drag data available for these wire mesh used in the GMRT antenna are an approximate of reality. Since the wire mesh accounts for the highest projected area in antenna structure, it would also account for the highest wind loads. Therefore a deeper analysis concerning the interaction of incoming wind with the wire mesh had to be done. Dr. Govind Swarup had published a paper [2] which has tabulated the coefficient of drag values for these meshes obtained theoretically and that through experimental aerodynamics at NAL. We compare the values given in [2] with that obtained through the application of CFD (Computational fluid dynamics). ANSYS Workbench and FLUENT were used for the CFD analysis of the wire mesh.

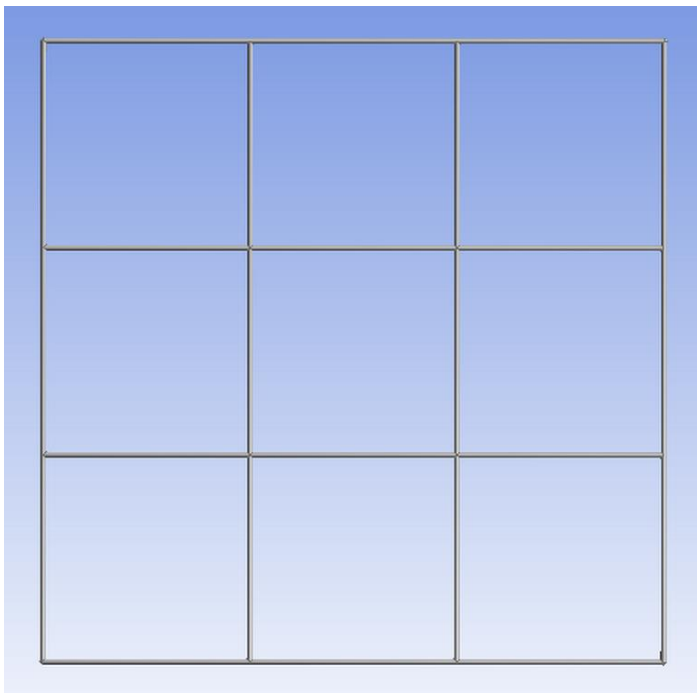


Figure 4

A small portion of the wire mesh was created using thin solid cylinders stacked together. The edges of the created wire mesh have been smoothed using spheres at the 4 corners of the wire mesh. Figure 1 shows the wire mesh created in the design modeller available in ANSYS Workbench for a 20mmx20mm mesh. A cuboid whose dimensions are way larger than that of the wire mesh was created to represent the fluid. The cuboid was frozen so to prevent the

interaction with the created wire mesh. A Boolean subtraction operator was created and the created wire mesh was subtracted from the cuboid. This empty space will be regarded as the wall during our analysis. The geometry was exported to “Mesher 13.0” which is the default workbench mesher for fluid dynamics.

An automatic meshing was applied to the imported geometry. The faces of the wire mesh wall were selected and a face sizing was applied. An element size of 0.01 mm was set. This element size was chosen because of memory constraints since FLUENT was crashing on elements any smaller than this. The mesher’s generate mesh feature was activated and the mesh was updated. The front face and the side faces of the cuboid were selected and were grouped into a named selection named “Far1”. The back face was selected and grouped as “Far2”. The wire mesh wall at the centre of the cuboid was selected and grouped into “wallmida” and “wallrestb”. Figure 2 shows the faces which have been grouped into wallmida and wallrestb. The middle square is the wallmida and the rest of the figure is grouped as wallrestb. The created data was updated and exported to FLUENT.

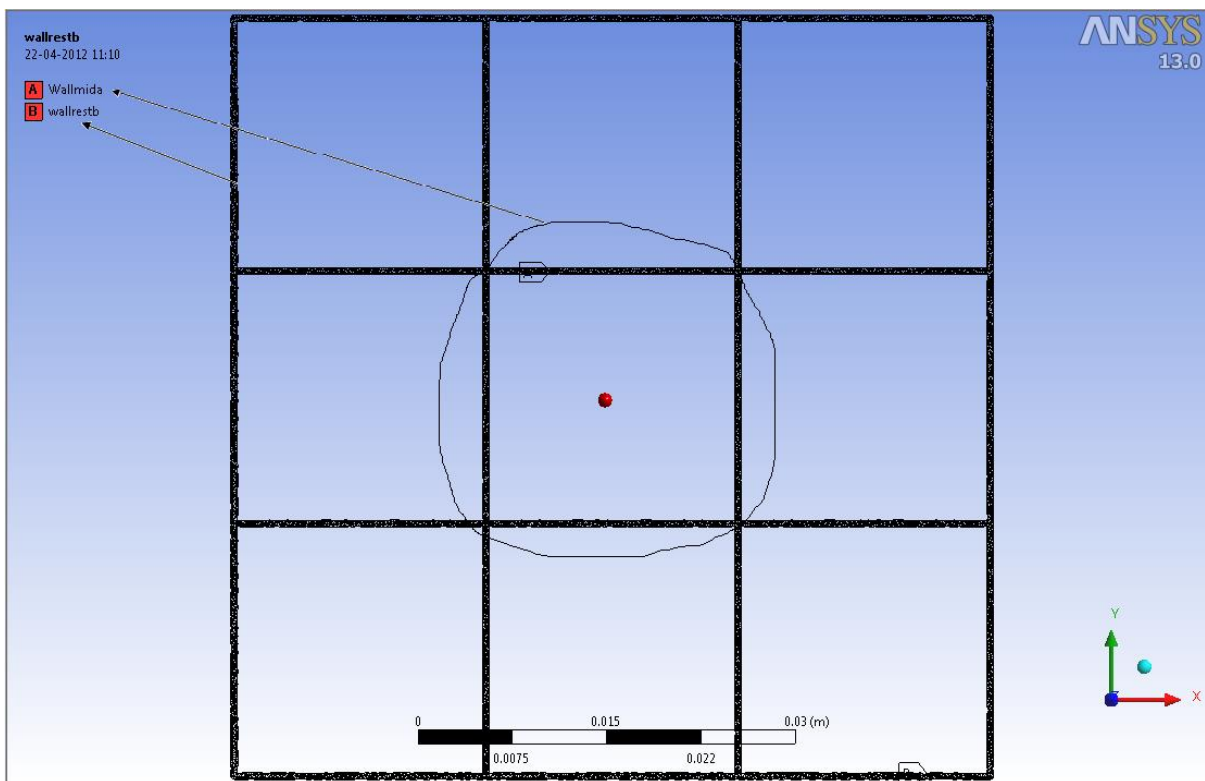


Figure 5

The imported mesh is checked for its quality and the minimum volume to ensure there are no elements with negative volume. The fluid in this scenario is air, hence the kinematic viscosity is set to $1.79 \times 10^{-5} \text{ m}^2/\text{s}$ and the density to $1.27 \text{ kg}/\text{m}^3$. The boundary conditions are set as velocity inlet with an appropriate incoming velocity for sections in far1, pressure outlet with a zero gauge pressure for sections in far2 and wall for section in wallmida and wallrestb. The monitors are set to show drag convergence data. The spatial discretisation used in this case was the “2nd order upwind scheme”. This scheme was chosen since it gives fairly accurate results when simulating a flow over a cylinder. Since the problem is closely similar, this scheme is assumed to give accurate results for flow over a wire mesh. The SIMPLE (semi implicit method for pressure linked equations) solver was used. The solution initialization is done with the data from “far1”. The number of iterations is set to 5000 and the solution is started. After the solution converges or after 5000 iterations, the report for the forces on “wallmida” and “wallrestb” for the direction vector that of the incoming velocity. The forces on the walls give the drag forces. This data is exported into excel and the coefficient of drag is calculated. The same is done for different Reynold’s number and different angles of attack and the forces on the wall in the direction of the flow and that perpendicular to it are noted and used to calculate the drag and lift coefficient.

$$C_D = \frac{\text{Force on the section obtained in a direction parallel to flow}}{\frac{1}{2} \rho_{air} V_Z^2 * \text{Area of the section projected on a plane parallel to the wire mesh}}$$

$$C_L = \frac{\text{Force on the section obtained in a direction perpendicular to flow}}{\frac{1}{2} \rho_{air} V_Z^2 * \text{Area of the section projected on a plane parallel to the wire mesh}}$$

The periodic boundary condition could not be applied on the model. Therefore a farfield boundary condition was applied to the side faces of the cuboid. Due to this there is a possibility of edge effects coming into the solution. Therefore the mesh was divided as shown in Figure 2 into one in the centre which has the least possibility of being effected by this and the rest of the mesh which have a higher possibility of being effected by this edge effect. Figure 3 shows the difference in modelling a finite mesh and an infinite one. The one on the left is a finite mesh. It can be seen that a small portion on each edge is exposed to the flow. This doesn’t happen in an infinite mesh since that portion continues. This small exposed portion which is about 1/18 the distance to the centre square can create vortices which may effect the flow field at the wake, thereby creating an extra drag effect. To eliminate the

possibility of this effecting the centre portion of the mesh a larger mesh has to be considered. Due to constraints in the configuration of the test rig, a large mesh could not be analysed. Hence an optimised size of the mesh had to considered.

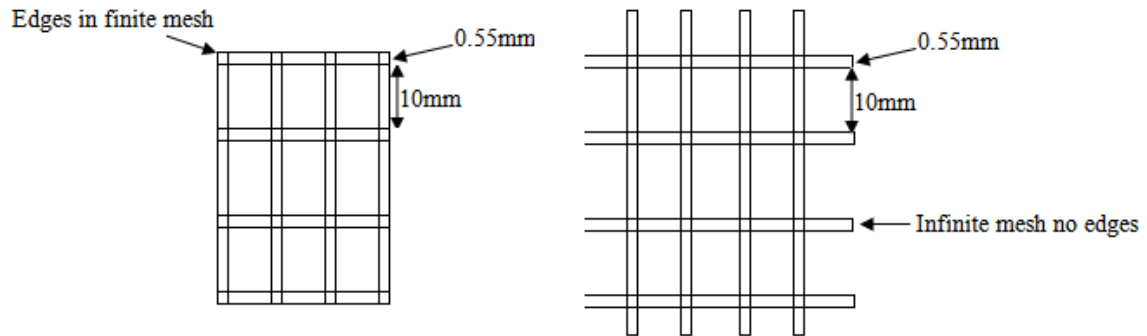


Figure 6: The difference between modelling a finite wire mesh (left) and an infinite one (right)

To calculate the size of the mesh beyond which the vortices created by the edges shown in Figure 3 would not effect the drag on the mid portion of the mesh a small CFD analysis was conducted. Cylindrical wires of 0.55mm diameter of different lengths were analysed to obtain the length beyond which the edge vortices won't effect the wake in the centre. These wires were simulated with the highest possible Reynolds number to account for the strongest edge vortices. The Coefficient of drag of these wires were tabulated and the length beyond which the coefficient of drag becomes constant can be considered to be the length beyond which the edge effects don't effect the centre of the wire. Since the edges in the wire mesh considered is very similar to those in the cylindrical wires, the same conclusion for the safe length can be extrapolated for the wire meshes.

2.2.8 CORROSION:

2.2.8.1 Model Information:

The members used in GMRT antenna are very thin. Due to this there has been a complete corrosion penetration in some of the members. At such areas there is a possibility for the presence of micro cracks from where damage can propagate into the whole member. Also such areas are prone to the concentration of stress where failure may occur. The effect of corrosion cannot be considered when modelling using beam/pipe elements since they assume that a member has constant cross section at every location.

To incorporate the effect corrosion can have on members modelled by pipe/beam elements, it was decided to amplify the stresses developed in the damaged members. To get an accurate value for this amplification factor, the corrosion damage was modelled by a circular through hole in the member. The area of the hole will be equal to the area on which complete corrosion penetration has taken place. Solid elements were used in the modelling since they can very accurately predict the local phenomenon.

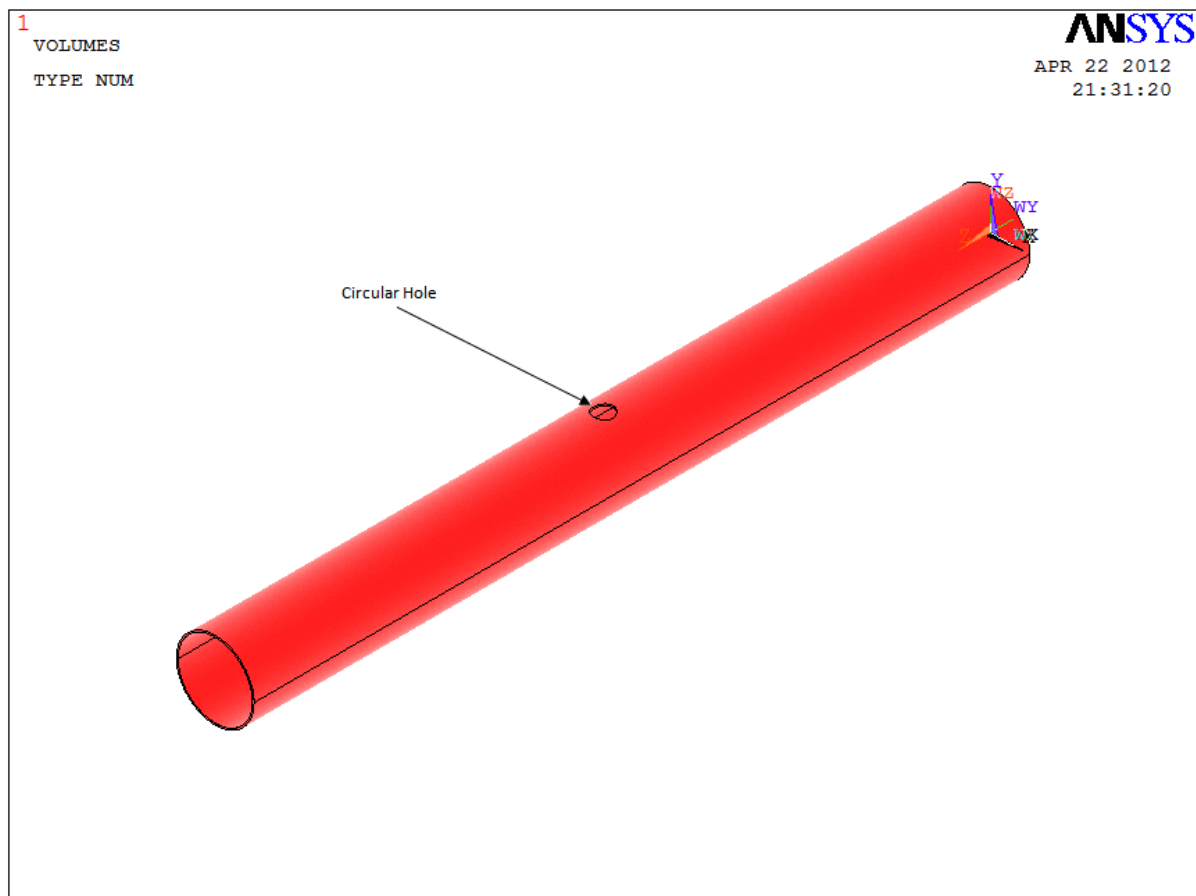


Figure 7: The model used to approximate corrosion

Figure 1 shows the model considered to depict corrosion. The factor by which the stresses amplified near the hole was calculated using this model. Since the antenna is a very huge truss structure it can be assumed with fair accuracy that the stresses developed in the members are purely tensile or compressive. The model has been analysed by applying a tensile force.

2.2.8.2 Modelling Methodology:

SOLID 285 elements were used for this modelling. These elements can depict the local phenomenon pretty well and hence were selected for the analysis. A hollow cylinder with radius equal to that of the member to be analysed is initially generated. A solid cylinder with radius equal to that of the hole and appropriate length is inserted inside the hollow cylinder as shown in Figure 2. The solid cylinder is inserted such that only it is in contact with the cylinder on only one side, the other end of the cylinder is inside the hollow cylinder.

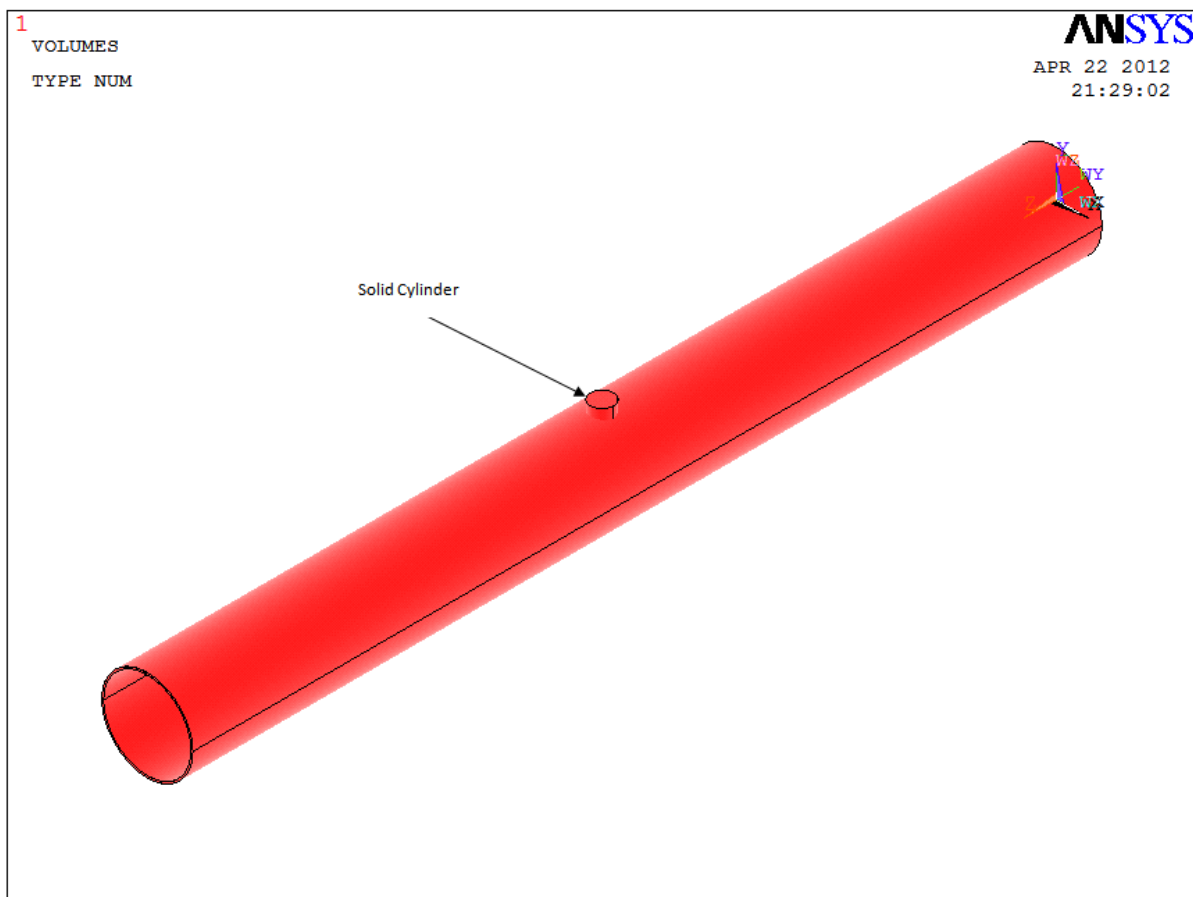


Figure 8: The position and orientation of the solid cylinder

A Boolean operator is used to subtract the solid cylinder from the hollow one, to create the model shown in Figure 1. The model is then sliced into many parts such that the elements can be concentrated near the hole. This is to model the hole with more accuracy and precision. Since the locations far from the hole are not very important in the analysis, a coarse mesh will be used to model them. The sliced model is shown in Figure 3.

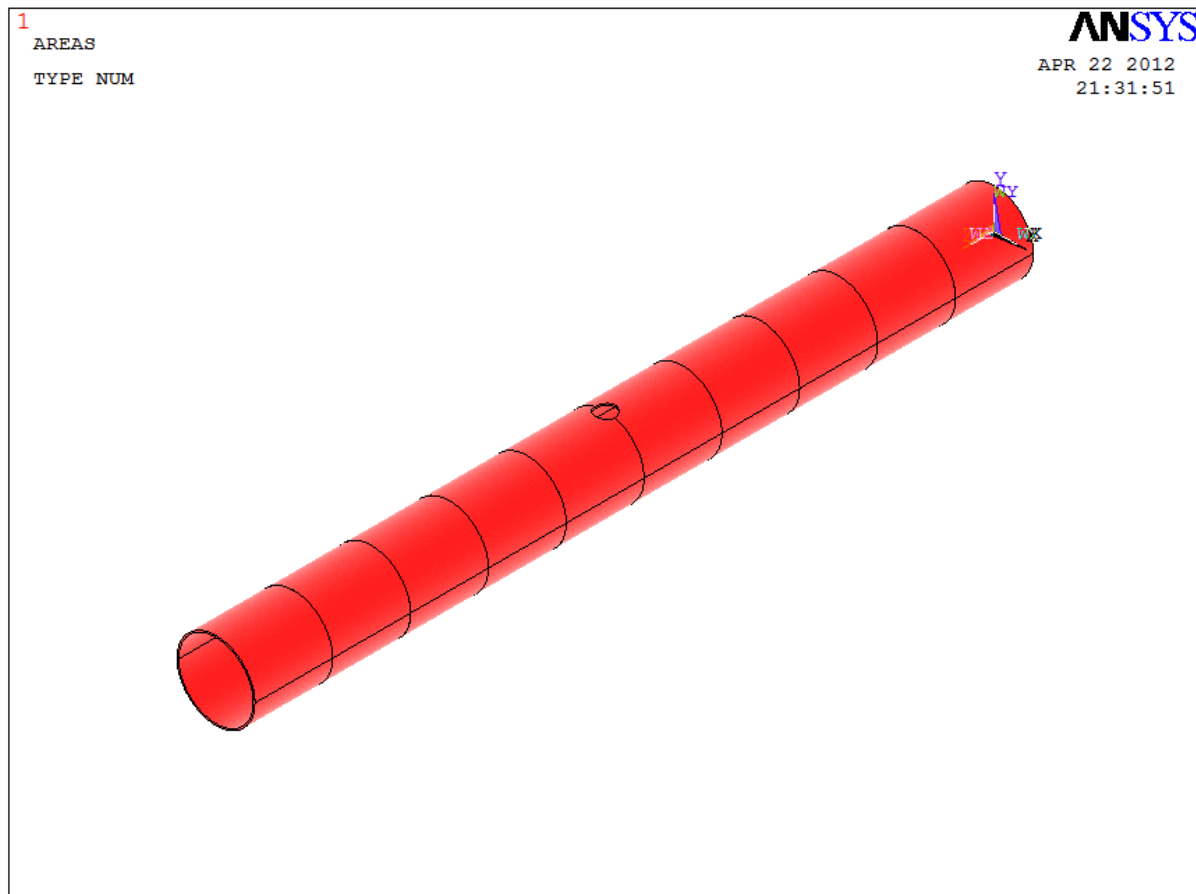


Figure 9

The Sliced model is glued together using a Boolean operator. The slices close to the hole and the ends are selected and are meshed using element size as 4. The other slices are then selected and meshed with element size 5. One end of the cylinder is fixed for all degree of freedoms. The other end is given a tensile load. Figure 4 depicts the meshed model. A static analysis is then conducted and the solution is started. The contour for the stress distribution is plotted and saved. The maximum developed stress are tabulated for different cylindrical members, hole sizes and locations. A path is created along the hole to check how the amplification of stresses takes place.

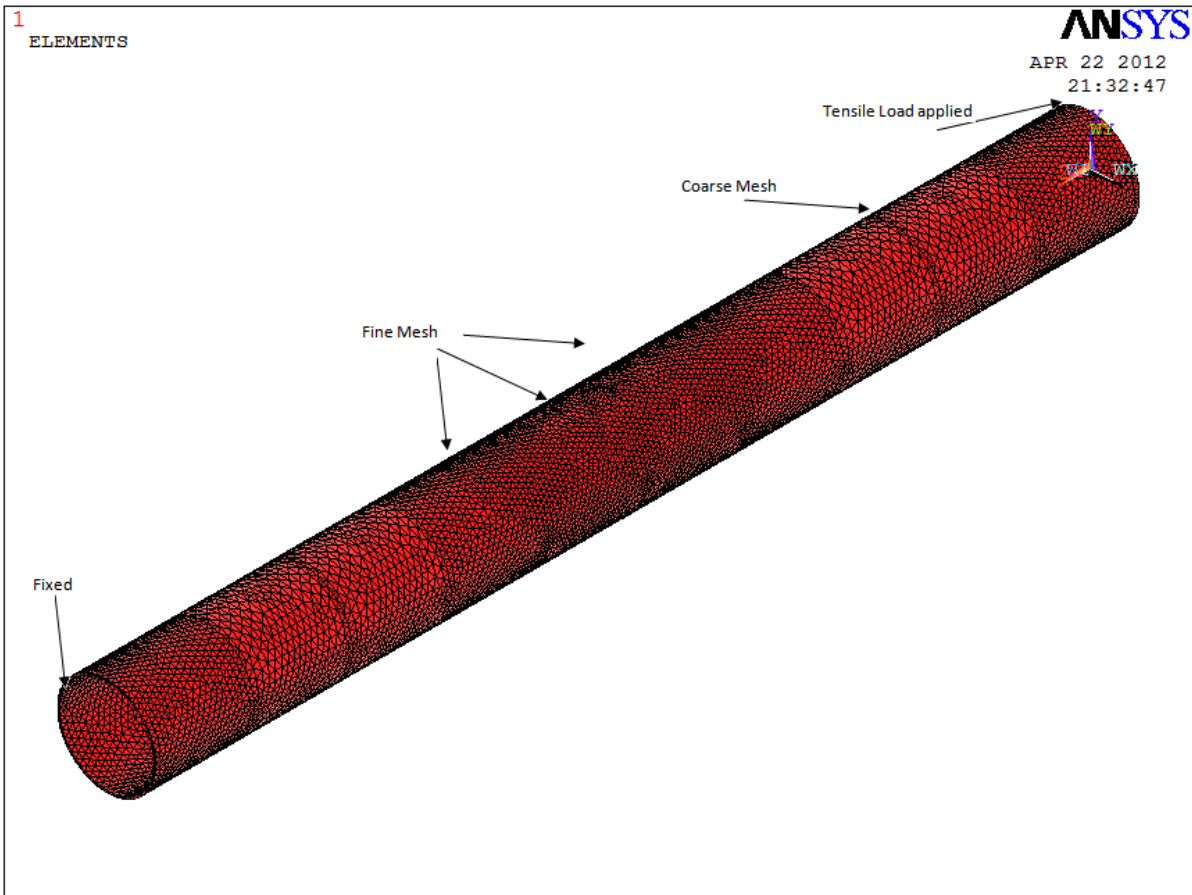


Figure 10: Model after meshing, showing the areas with fine and coarse mesh

3. Results and discussions

3.1 ANSYS WORKBENCH RESULTS

3.1.1 Cylindrical wire:

The CFD analysis was done in FLUENT using 2nd order upwind scheme. The results were tabulated and plotted. Table 1 shows the results of the analysis done on the cylindrical wire. It shows the variation of C_D for the whole wire with length. The force on the wire obtained from FLUENT has been input into excel and the coefficient of drag has been calculated by dividing force obtained with the product of incoming dynamic pressure and projected area.

Length of the wire (mm)	Dynamic pressure *projected area (N)	Force (N)	C_D
45	0.024354	0.020321883	0.834437177
60	0.032472	0.027692789	0.852820553
75	0.04059	0.034861612	0.858871939
90	0.048708	0.041064113	0.843067114
105	0.056826	0.047217586	0.83091518
120	0.064944	0.055474548	0.854190503
135	0.073062	0.062374573	0.853721127

Table 4: Variation of the Force on the mesh and C_D with the length of the wire

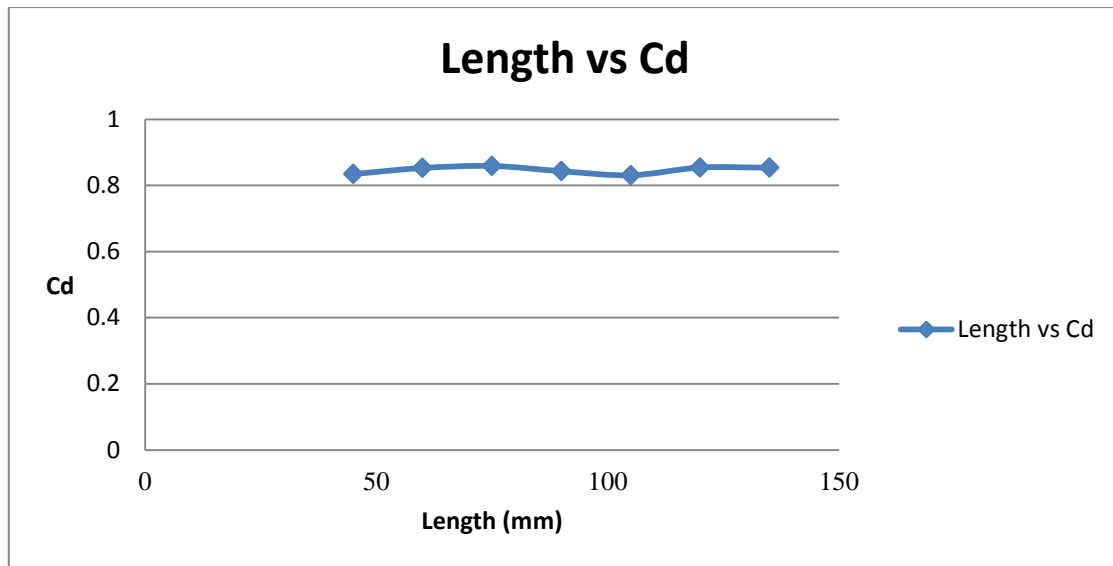


Figure 11: Variation of C_D with the length of the wire

Figure 1 depicts the variation in C_D with the length. It can be noticed from Table 1 and Figure 1 that there has been no significant change in the value of C_D . It can be concluded from this that the effect of the edges in the finite mesh is nearly negligible since the C_D for a very long wire is nearly the same as that for a short one. Hence, the edges effects on the considered wire mesh viz. 10mmx10mm, 15mmx15mm and 20mmx20mm will be very negligible and can be neglected with sufficient accuracy when considering lengths over 45mm.

3.1.2 CFD on Wire Mesh:

Based on the results obtained from the analysis on the cylindrical wire, the wire meshes, 10mmx10mm, 15mmx15mm and 20mmx20mm were analysed by considering lengths of 50mm, 45mm and 60mm respectively. The lengths were chosen because it was concluded that there would be sufficient accuracy in the results when considering lengths over 45mm. Table 2 shows the variation in C_D with solidity and Reynold's number.

Mesh type	Solidity	Inflow velocity (m/s)	Re	Force (N)	C_D	C_D measure d (NAL) [2]
20x	0.0	4	12	0.040	0.969	0.
20	54	0	30	658	568	98
20x	0.0	3	92	0.023	0.982	0.
20	54	0	2	164	005	98

20x	0.0	2	61	0.010	0.991	0.
20	54	0	5	394	42	98
20x	0.0	1	46	0.005	1.001	0.
20	54	5	1	907	759	98
15x	0.0	4	12	0.031	1.022	1.
15	72	0	29	85	336	07
15x	0.0	3	92	0.017	1.026	1.
15	72	0	2	982	136	07
15x	0.0	2	61	0.008	1.034	1.
15	72	0	5	06	908	07
15x	0.0	1	46	0.004	1.042	1.
15	72	5	1	569	881	07
10x	0.1	4	12	0.021	1.039	-
10	07	0	29	174	263	
10x	0.1	3	92	0.012	1.050	-
10	07	0	2	035	105	
10x	0.1	2	61	0.005	1.055	-
10	07	0	5	374	085	
10x	0.1	1	46	0.003	1.062	-
10	07	5	1	045	727	

Table 5: Variation of C_D with Solidity and Reynold's number

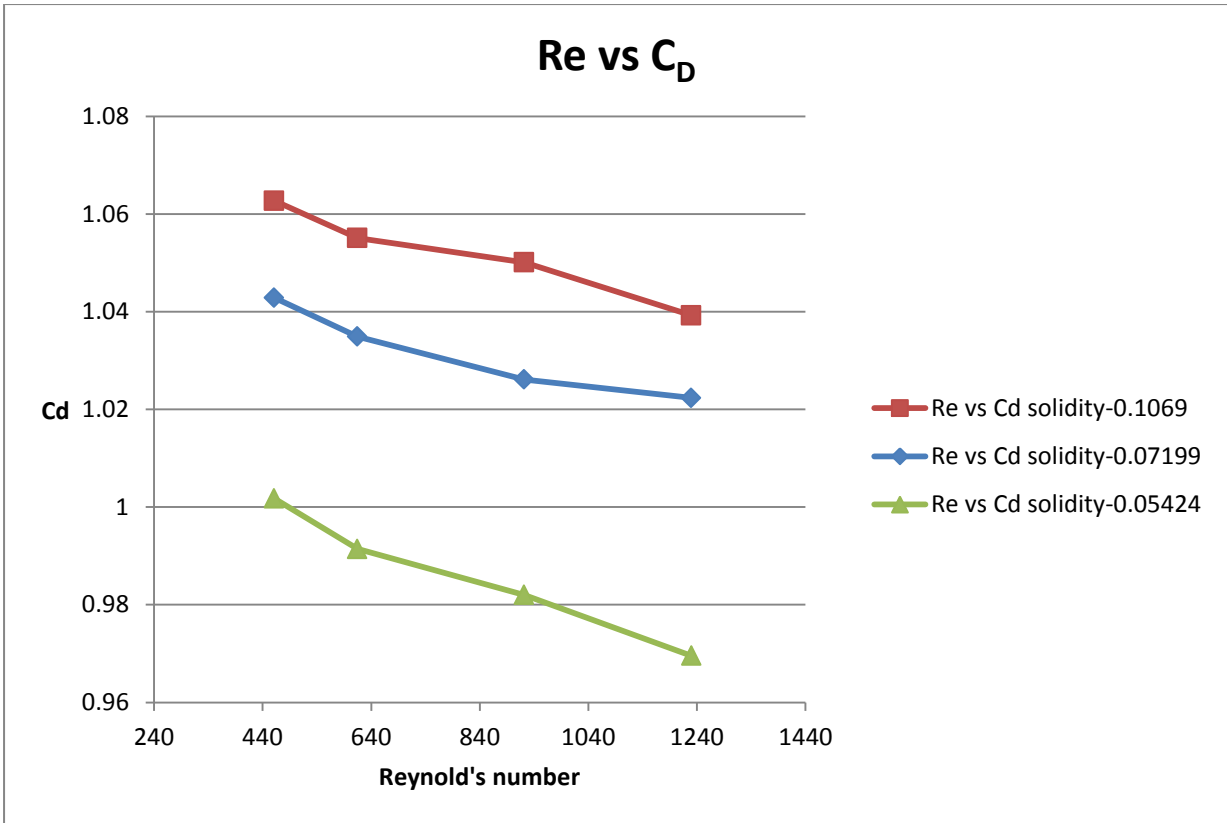


Figure 12: Variation of C_D with Reynold's number for different solidity

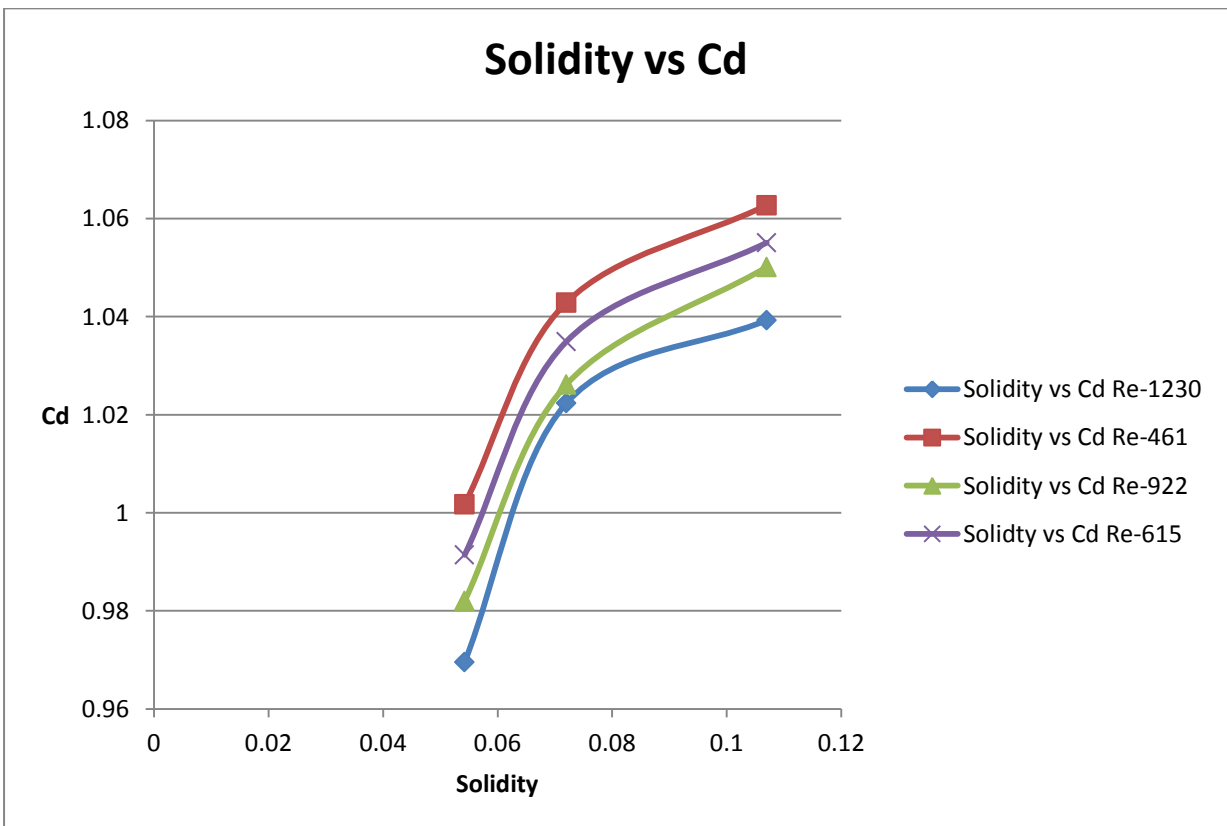


Figure 13: Variation of C_D with solidity for different Reynold's number

The values for the coefficient of drag obtained from the CFD analysis on the wire meshes are very close to the values measured in wind tunnel experiments conducted by NAL as given in Dr. Govind Swarup's paper [2].

The decrease in C_D with an increase in Reynold's number is consistent with the theoretical prediction. This is expected to be due to the increase in the momentum of the incoming flow as compared to the viscous forces. Due to this the flow becomes less laminar, though at such low Reynold's numbers it is not quite evident of the effect on the laminar flow.

The increase in C_D with an increase in solidity is consistent with that predicted theoretically. This is expected to be due to the relative increase in the exposed area. This is found to be consistent with that predicted theoretically in [2].

The wire mesh was also simulated for different angle of attack. The variation of force coefficients with angle of attack is plotted in Figures 4-6.

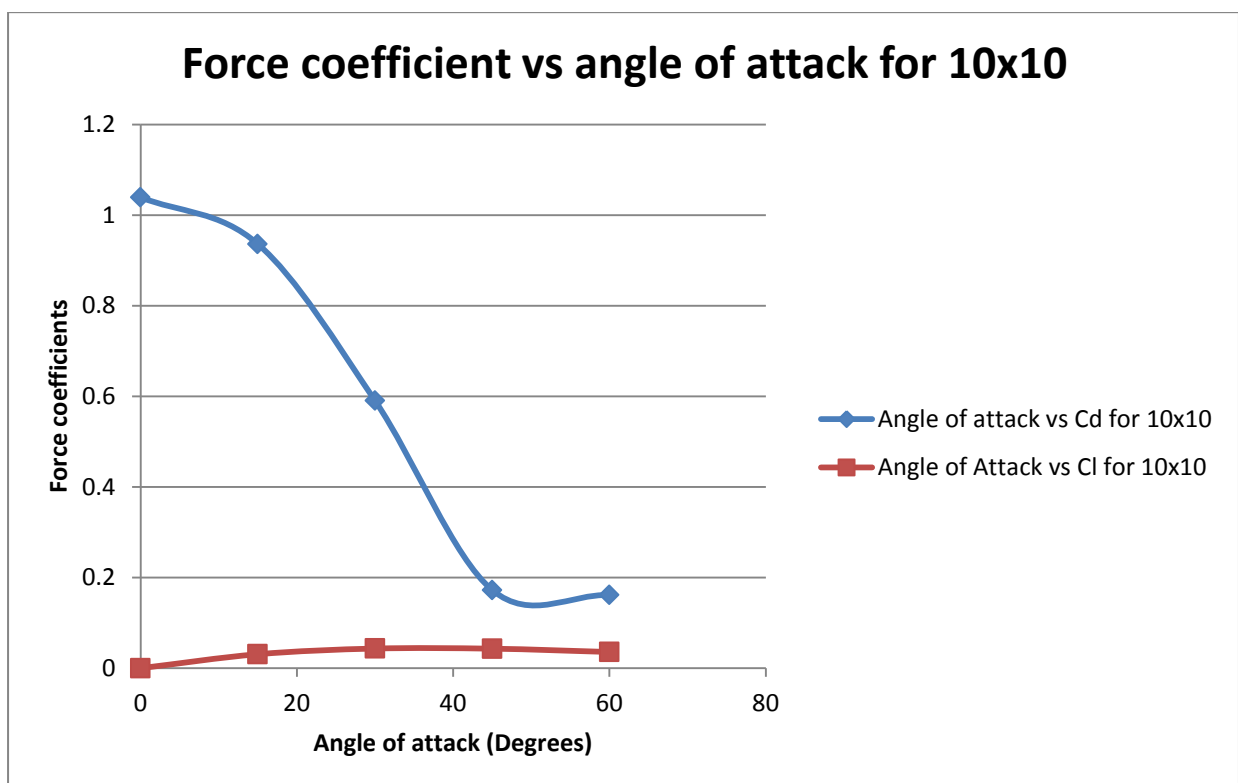


Figure 14: Variation of force coefficients with angle of attack for 10x10mm mesh

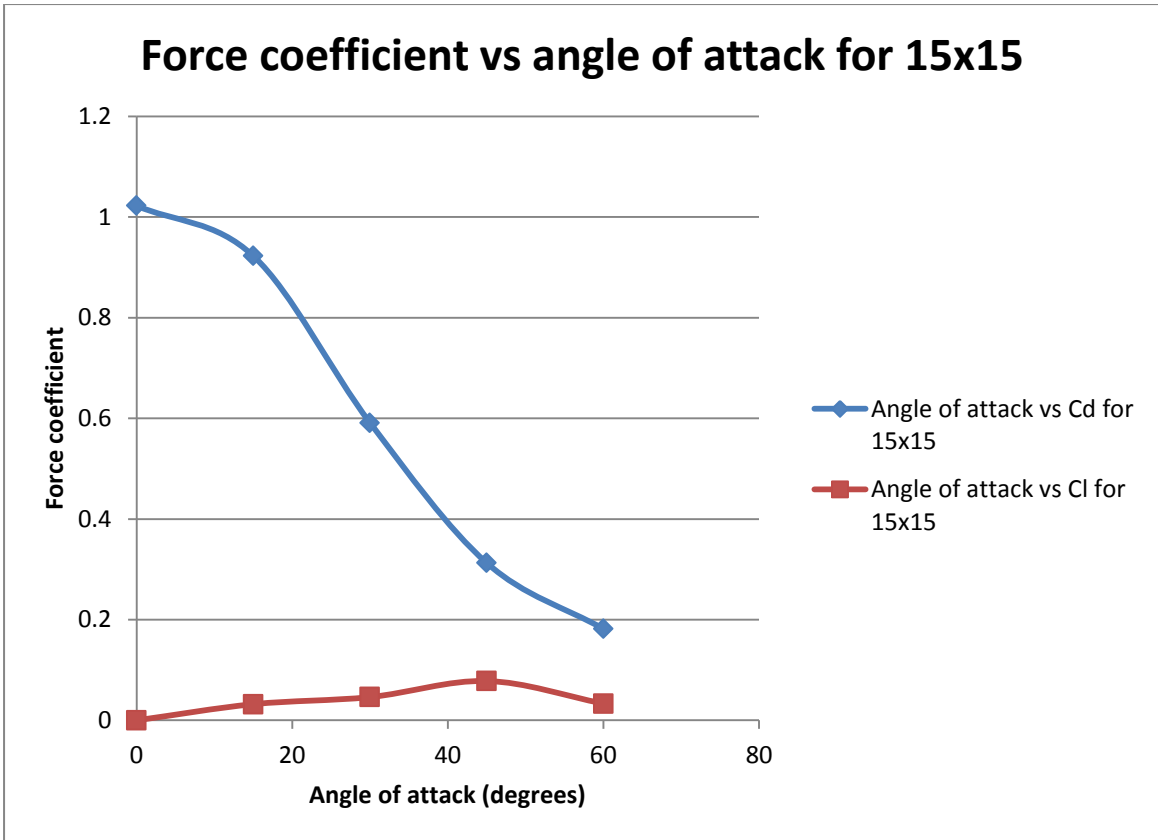


Figure 15: Variation of force coefficients with angle of attack for 15x15mm mesh

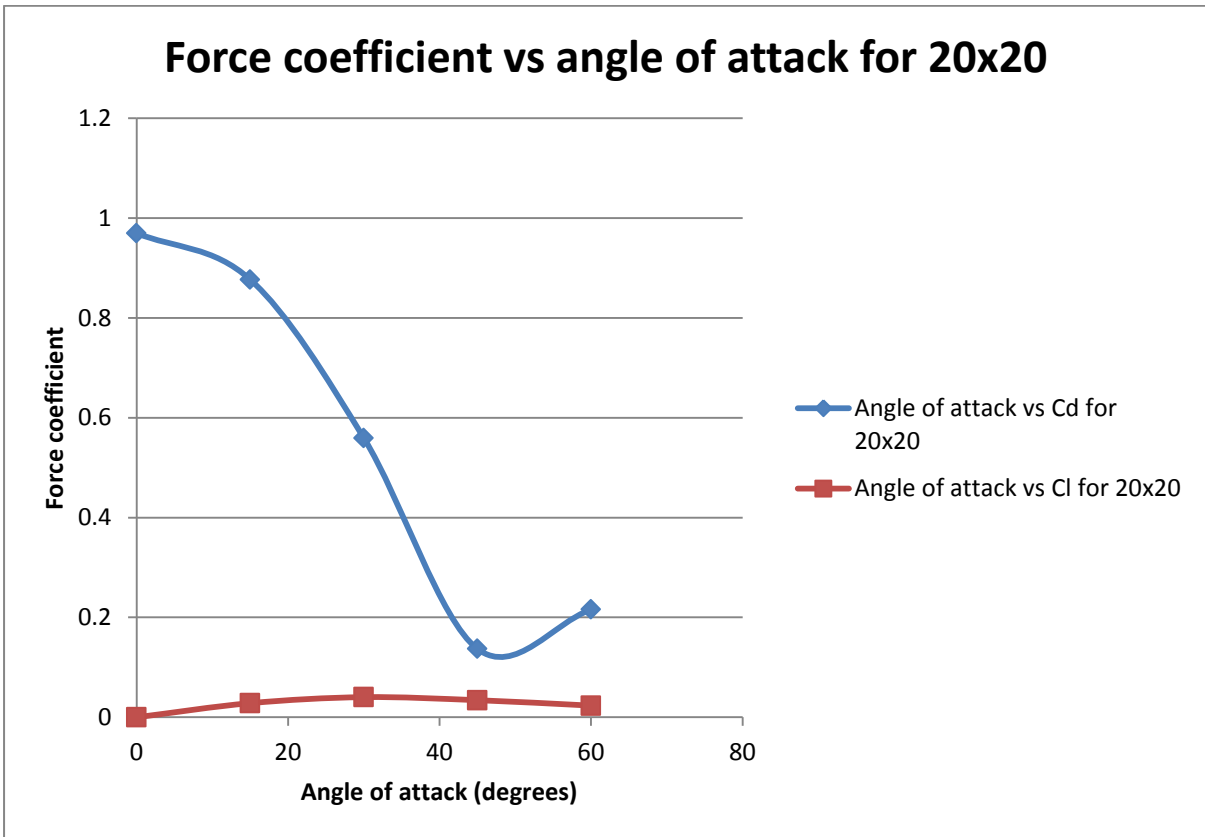


Figure 16: Variation of force coefficients with angle of attack for 20x20mm mesh

The trend followed by drag and lift coefficients is similar to that mentioned in Dr.Govind Swarup's paper [2]. These coefficients have been used in the calculation of wind forces on mesh.

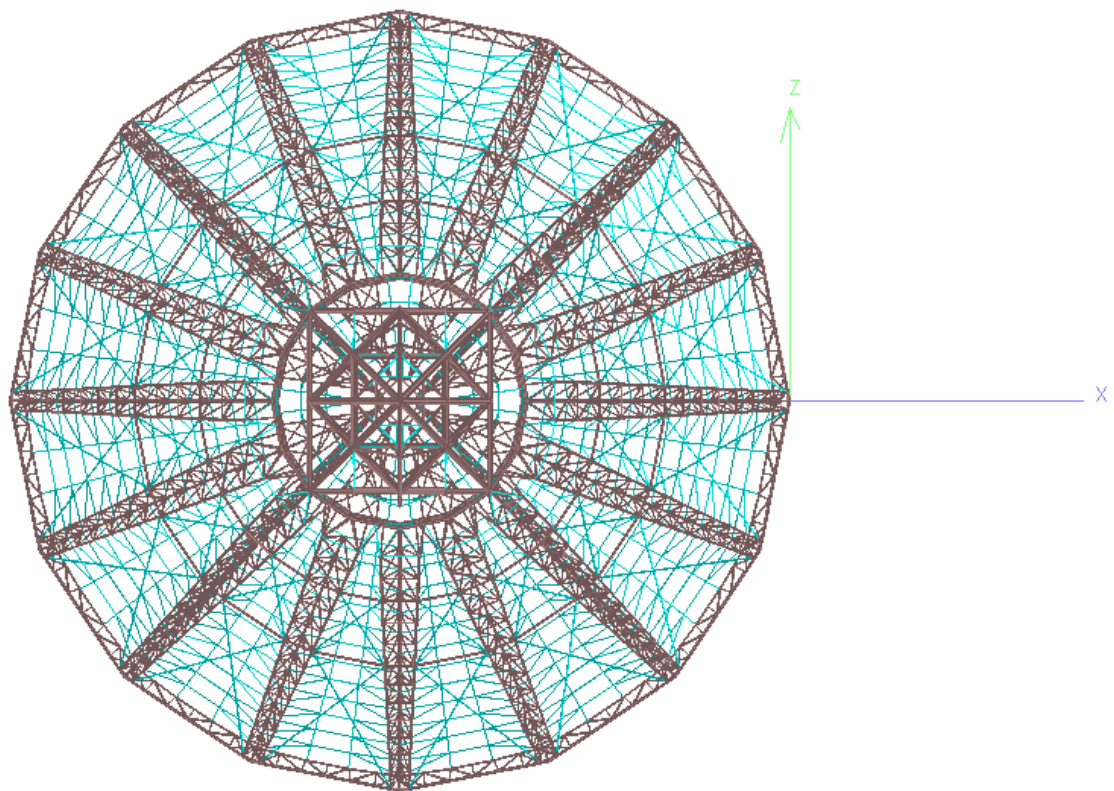
3.2 STAADPRO V8i RESULTS

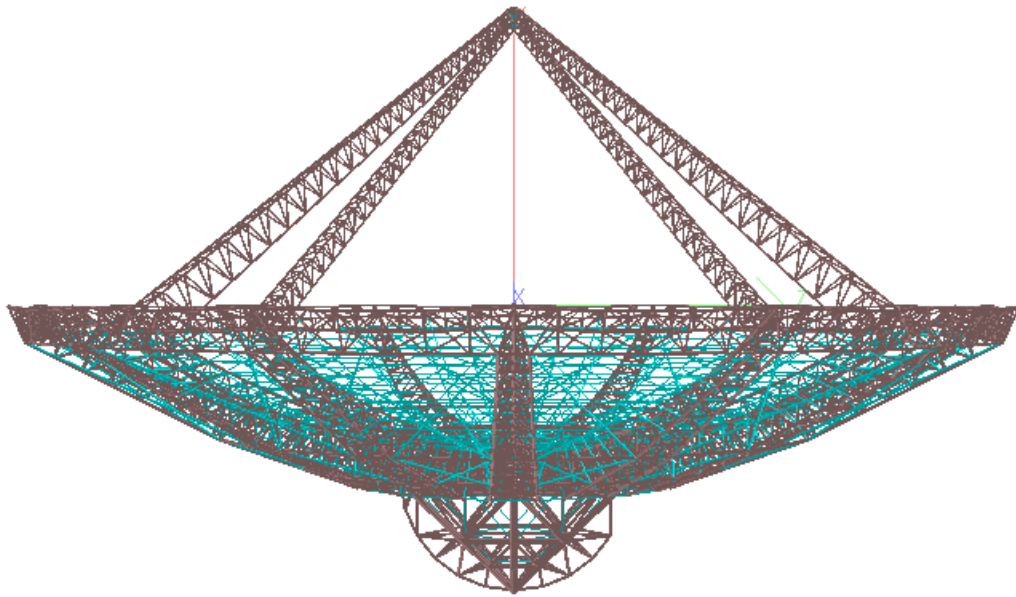
3.2.1 Finite element model

The FEM model is a space frame structure consisting of 6363 members and 2284 nodes. All the tubular sections are modeled as beam members.

The finite element model consists of

- 16 PRFs (3 types)
- The cradle with counter weight
- The Rim
- The Hub
- The quadripod and the cage support truss





The yoke and the supporting pillar are not considered. The lightning arrestors are not modeled; however their weights have been appropriately compensated in the dead weight.

3.2.1.1 Coordinate system

A right handed Cartesian coordinate system is used. The global X and Z axes are in the horizontal plane and the global Y axis is vertical and points upwards. The X- Axis is along the elevation axis.

3.2.1.2 Rope truss system

The wire ropes used in the structure are of different sizes namely, diameter 4.0 mm, 2.0 mm and 1.5 mm. These wire ropes are subjected to a pretension load. Due to the modelling and analysis constraints the diameter of the wire ropes (circumferential, radial and pulling wire ropes)) used in the model is 4 mm. The increase in dead load of wire ropes on dish structure (due to higher diameter) is negligible.

3.2.1.3 Cross bracing system

Cross bracing system, with 32 /28 mm diameter rods, is provided in each of the outer sixteen sectors of the dish structure. These Bracings are defined as tension members in the STAAD model, so that it will be active only when these members are in tension. Pre-tension force of about 3000 Kg. is considered in the bracing.

3.2.1.4 Boundary conditions

The dish is supported on nodes at the elevation bearing locations. The x, y and z displacement of one end of elevation axis node are restrained along all 3 directions. The node at other end

of elevation axis is restrained along X and Y directions. This boundary condition is kept similar to that given in earlier analysis in SHL1. Rotations about X, Y and Z axes are free

3.2.2 Dead load case

3.2.2.1 Configuration:

- Yield strength of YST-210 steel: 215 MPa
- Elevation angles: -20, 0, 15, 30, 45, 75, 90
- L1: Feed loads(kg): 700,1000,1100,1300
- L2: Dead load: $g = 9.81 \text{ m/s}^2$ (-GY)
- L3: Counterweight : 400 KN
- L4: Pretension load: 3000kg on cross bracings
- L5: Repeat Load: $L1 + 1.1X L2 + L3 + L4$

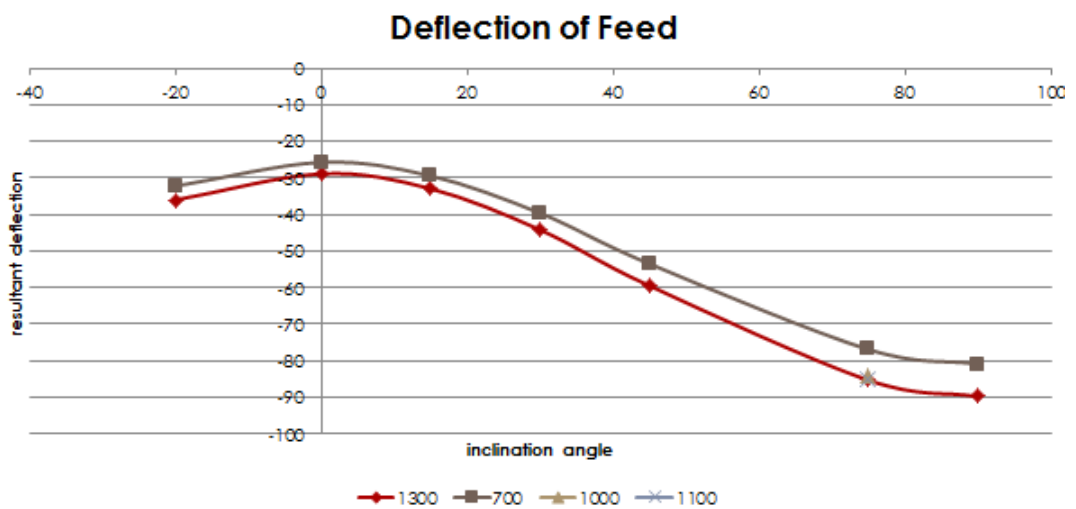
3.2.2.2 Maximum stress ratio reached for Feed load = 1300 kg

The stress ratios are plotted against the members where the absolute stress value exceeds 100 MPa. **The relevant plots are included in the appendix.** 1300/DD/-20 signifies 1300 kg feed load, no wind load, and inclination angle as -20 degrees. The numbers below the node title identifies the corresponding member in the model. From the following tables we note that the stress ratio doesn't exceed 1 as required.

Inclination angle	Maximum stress ratio reached in the structure
-20	.85
0	.74
15	.82
30	.83
45	.86
75	.71

3.2.2.3 Deflection of feed under different orientation for feed load =1300 kg

Feed load(kg)	Inclination of dish from zenith	Feed deflection (mm)
700	75	78.058
1100	75	83.85
1200	75	84.98
1300	75	86.60



3.2.2.4 Inference

- Maximum stress achieved is around .8YLD.
- They slightly vary with the TCE stress values.
- The feed deflection values are higher than the TCE values.

3.2.3 Wind load case

3.2.3.1 TCE vs. TWL

As we mentioned before we have used two methodologies to apply the wind loads; the TCE methodology and the TWL (true wind load) methodology. As the TCE methodology is an over approximation the wind loads on the members are higher and hence the deflections are larger.

The following table clearly compares deflection data for both methodologies when the wind speed is 140kmph which is the highest wind speed in the Nashik region as per to IS: 875

wind code. These values represent the individual maximum values of along each axis and the resultant.

Wind speed		140 KMPH		
TWL loading	x	y	z	resultant
	87.444	-66.442	-17.323	97.864
TCE loading	x	y	z	resultant
	152.24	-30.706875	-0.03675	156.39

3.2.3.2 Operating wind speed

The maximum operating wind speed for the GMRT antenna is 40 kmph. Thus, if for this wind speed the antenna stress ratios remain under 1, then we can safely conclude that the antenna can safely operate under this speed.

We would like to mention that we have only considered static conditions, whereas in the real world scenario the antenna is subjected to dynamic loadings.

The analysis was carried out for inclination angles for 0, 45, 60, 75 degrees from the vertical axis. The stress ratio for the maximum stressed members did not exceed 1.

3.2.3.3 Analysis for Maximum wind speed in Nashik region 140 kmph

At speeds over 40 kmph the antenna automatically parks itself at its zenith looking position. Thus this analysis is done only for zero inclination angle. The plots are in the included DVD.

It should be mentioned here that a single anomaly was spotted here. A member belonging to the top part of quadripod has a stress ratio exceeding one. This may be due to the absence of a load bearing plate element in our model as compared to the real structure.

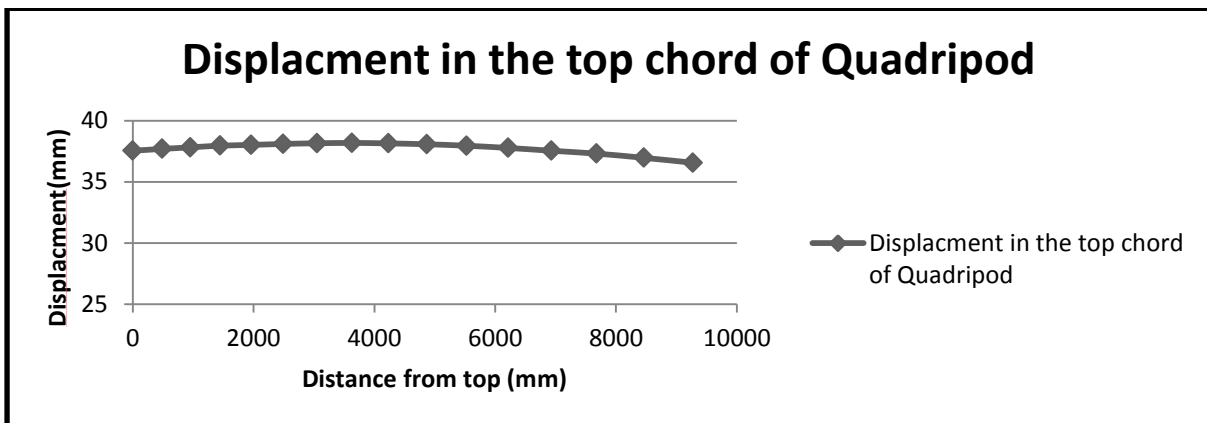
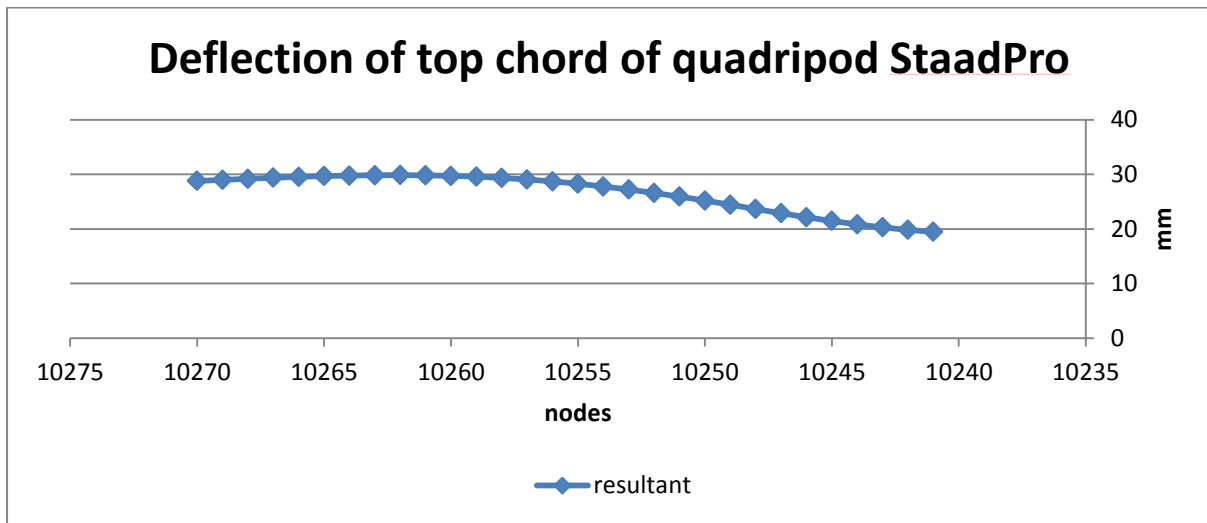
3.2.3.4 Analysis for survival wind speed

3.2.4 Ansys Mechanical vs. Staad.Pro V8i

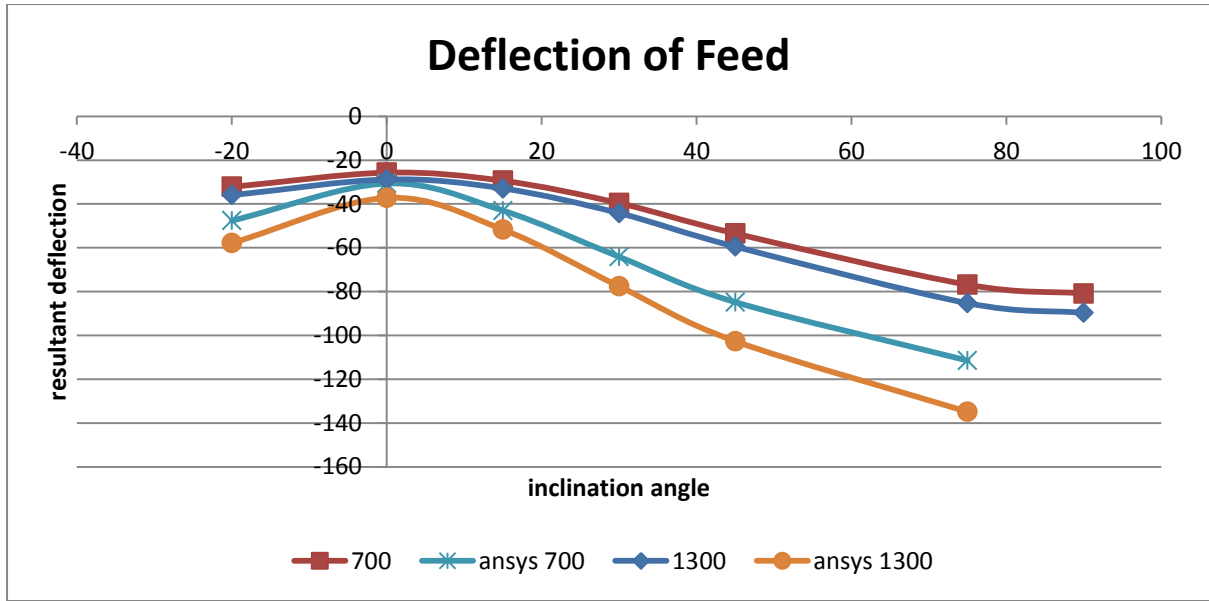
3.2.4.1 Configuration

- Zenith looking position of dish
- L1: Feed loads(kg): 1300
- L2: Dead load: $g = 9.81 \text{ m/s}^2$ (-Y)
- L3: Counterweight: 400 KN
- L4: Pretension load: 3000kg on cross bracings
- L5: Repeat Load: $L1 + 1.1 \times L2 + L3 + L4$

The following plots compare the deflection of top chord of quadripod for the two packages. As we can see the deflection values for Ansys are on the higher side.



The plot below compares the deflection values of the feed under feed loads of 700kg and 1300kg. Here too, Ansys Mechanical gives values on the higher side compared to Staad.Pro.



3.3 ANSYS MECHANICAL RESULTS

A static analysis on the antenna was conducted on the antenna. The variation of displacement of the feed with the inclination of the antenna due to dead weight for a feed weight of 1300kg has been tabulated in Table 1.

Feed weight - 1300 kg				
Inclination	Displacement (mm)			
	X	Y	Z	Resultant
-20	-3.95E-05	-35.07	46.002	57.84539
0	1.05E+00	-37.224	1.134	37.25598
15	1.99	-36.709	36.324	51.68117
30	2.78	-34.47	69.49	77.61939
45	3.572	-	97.963	102.667
		30.5122		
75	4.66	-	133.529	134.9124
		18.6987		

Table 6: Variation of displacement of feed at different inclinations of antenna for feed of 1300kg

The displacement of the feed due to dead weight when there is no feed has been tabulated in Table 2.

NO FEED				
Inclination	Displacement (mm)			
	X	Y	Z	Resultant
-20	-4.30E-05	-28.82	-37.92	47.62897018
0	1.00E-01	-30.667	0.8	30.67759588
15	2.11	-30.617	30.157	43.0267061
30	2.67	-28.7133	57.283	64.13208702
45	3.385	-25.8075	80.7221	84.81475526
75	4.346	-16.947	110.128	111.5090351

Table 7: : Variation of displacement of feed at different inclinations of antenna for no feed

The variation of displacement with the inclination of the antenna has been plotted in Figure 1. The data has been plotted considering only dead weight. Figure 2 shows the variation in the displacement of the nodes on the top chord of the Quadripod.

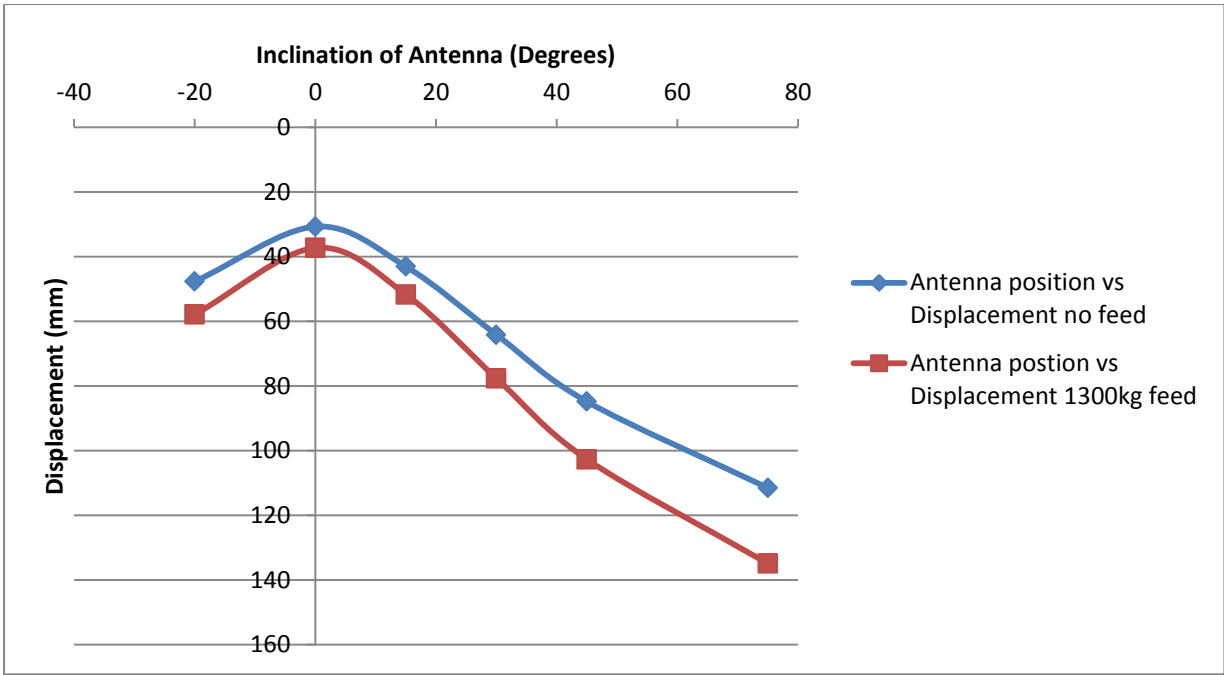


Figure 17: Variation of displacement with different inclinations of antenna

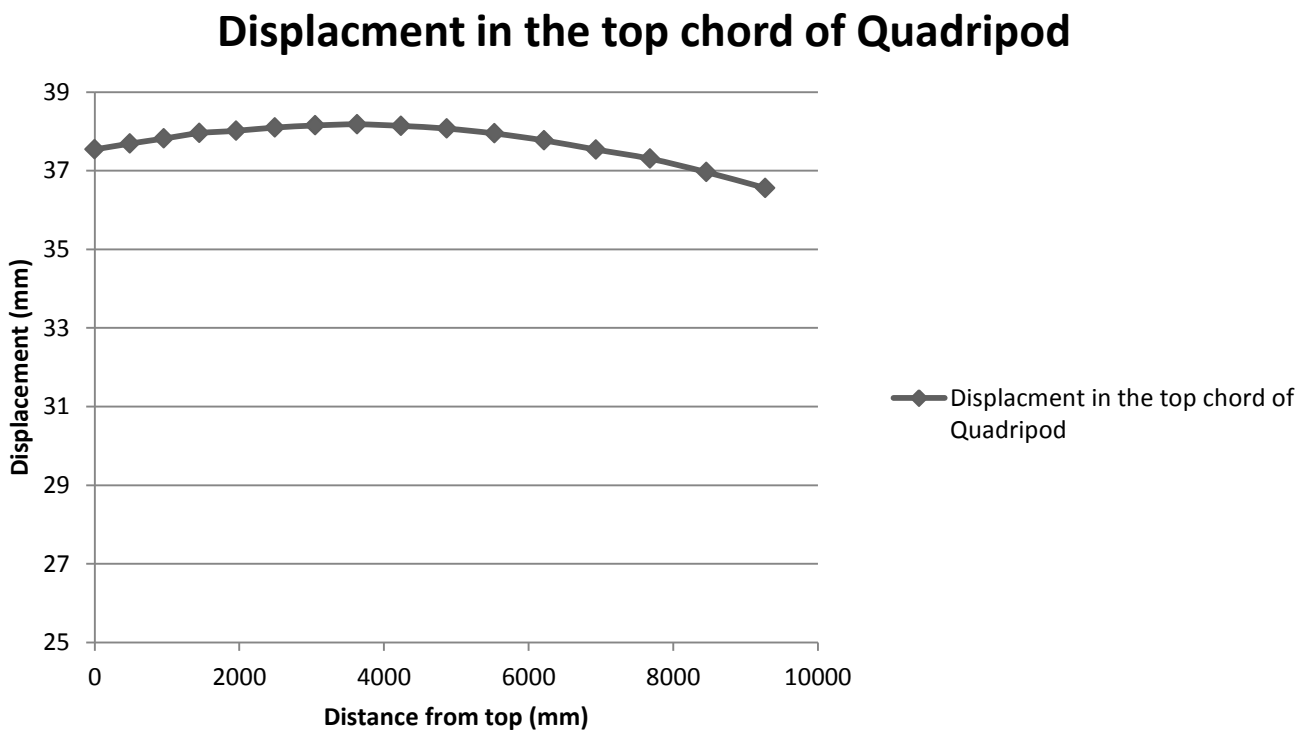


Figure 18

Figures 3-5 depict the variation of displacement on different locations of the antenna structure. These figures have been colour coded for better visualisation.

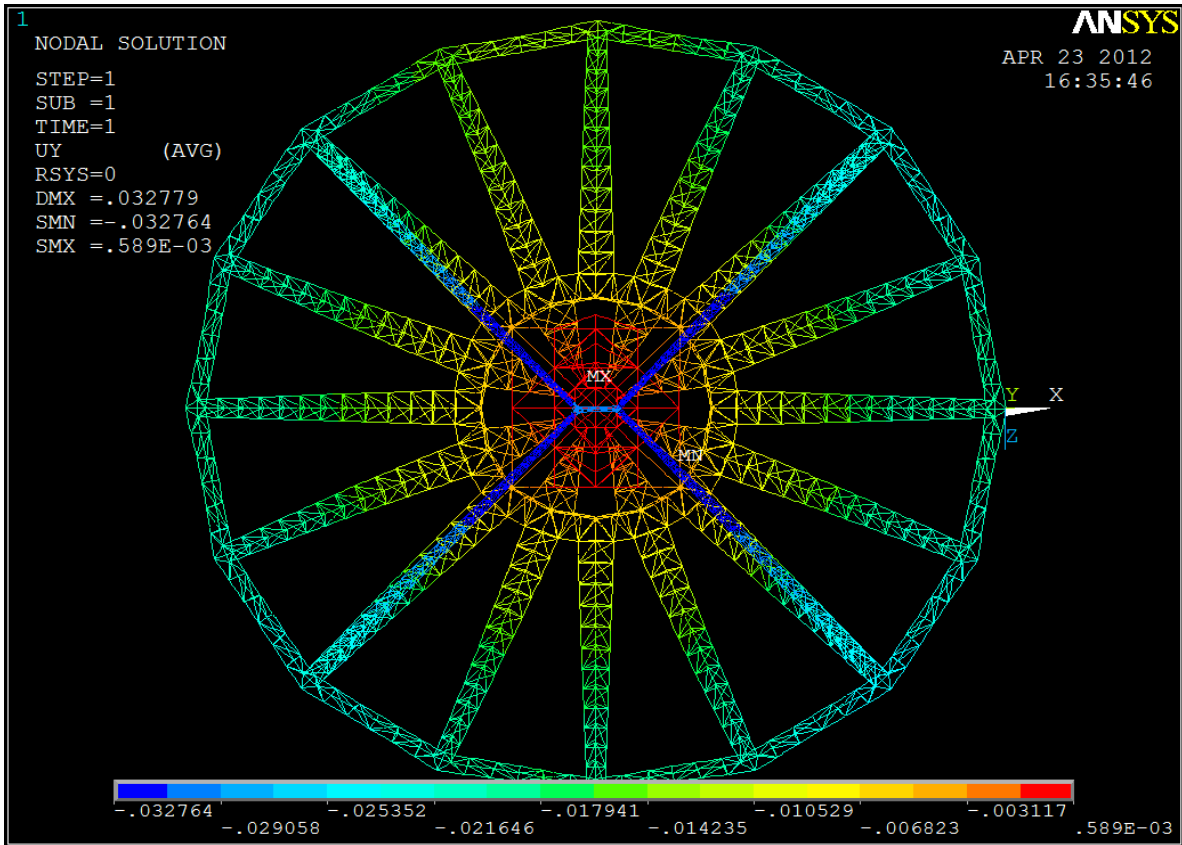


Figure 19 : Variation of displacements at different locations in the antenna when the dish is facing the sky.

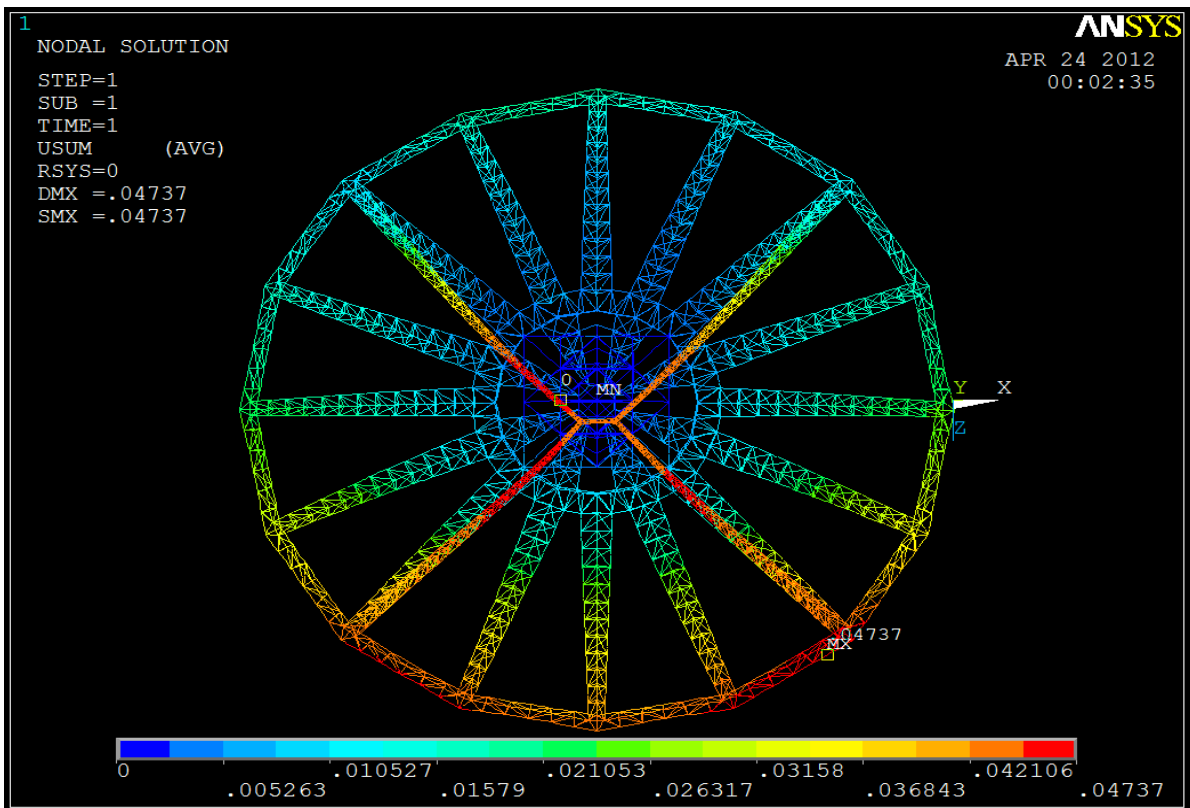


Figure 20: Variation of displacements at different locations in the antenna when the dish is facing 15 degrees forward.

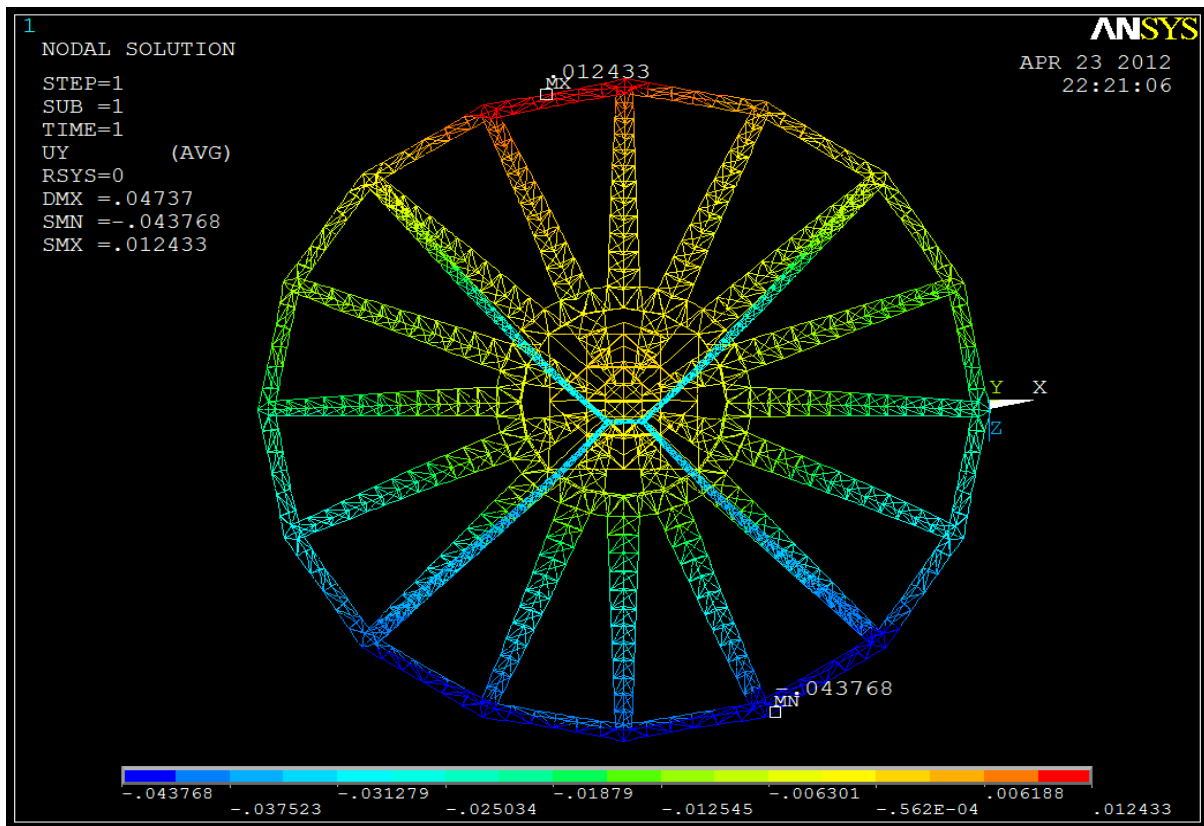


Figure 21 : Variation of displacement at different locations of antenna when the dish is facing 20 degrees backward.

3.3.1 Inference

It has been noticed that the values for displacement obtained in ANSYS are way larger than that obtained through STAADPRO. Though the trend for the change in displacement with inclination of antenna is the same. At inclinations close to the zenith the displacement values obtained in ANSYS are very close to that in STAAD. At higher inclinations the displacements obtained in ANSYS are nearly 50% more than that obtained through STAAD. Since, the model is exactly the same in both ANSYS and STAAD, such a large difference in values is counter intuitive. The reason for this variation is not yet known but is expected that this may be due to the difference in how ANSYS and STAAD deal with large displacements.

It can be noticed that the displacements at different locations in the antenna is quite intuitive. The variation is symmetric and as predicted. The nearly asymmetric contour in figure 5 as compared to figure 4 is as expected since the dish is facing the opposite sides. An asymmetry can be noticed in the top portion of the rim in figure 5, this is counter intuitive since the structure and loading are perfectly symmetric about the Z-axis. The reason for this asymmetry is not know of yet.

The values of stress at different locations could not be obtained because of memory constraints.

3.4 ANSYS CORROSION RESULTS:

An approximation of corroded members was done considering a hole drilled through the members. It was modelled in ANSYS using Solid elements. Table 1 gives the amplification factor for different hole sizes and thickness for a beam of outer diameter 100mm.

Outer Diameter(mm)	Thickness(mm)	Hole size (mm)	Amplification factor
100	2	20	2.84E+00
100	2	25	2.92E+00
100	2	30	3.41E+00
100	2	35	3.67E+00
100	2	40	3.73E+00
100	3	20	2.64E+00
100	3	25	2.90E+00
100	3	30	3.33E+00
100	3	35	3.48E+00
100	3	40	3.72E+00
100	4	20	2.66E+00
100	4	25	2.82E+00
100	4	30	3.28E+00
100	4	35	3.44E+00
100	4	40	3.84E+00
100	5	20	3.08E+00
100	5	25	3.24E+00
100	5	30	3.54E+00
100	5	35	3.66E+00
100	5	40	3.91E+00
100	6	20	3.12E+00
100	6	25	3.42E+00
100	6	30	3.52E+00
100	6	35	3.67E+00
100	6	40	4.03E+00

Table 8: Variation of amplification factor with thickness and hole size

Figures 1-3 show graphically the variation of stresses near the hole for different hole sizes. The X-axis represents the distance along a circular path passing through the hole and the Y-axis represents the stresses. Figures 4 and 5 show the stress distribution near the hole. Figures 6 and 7 plot the variation of amplification factor with hole size and thickness.

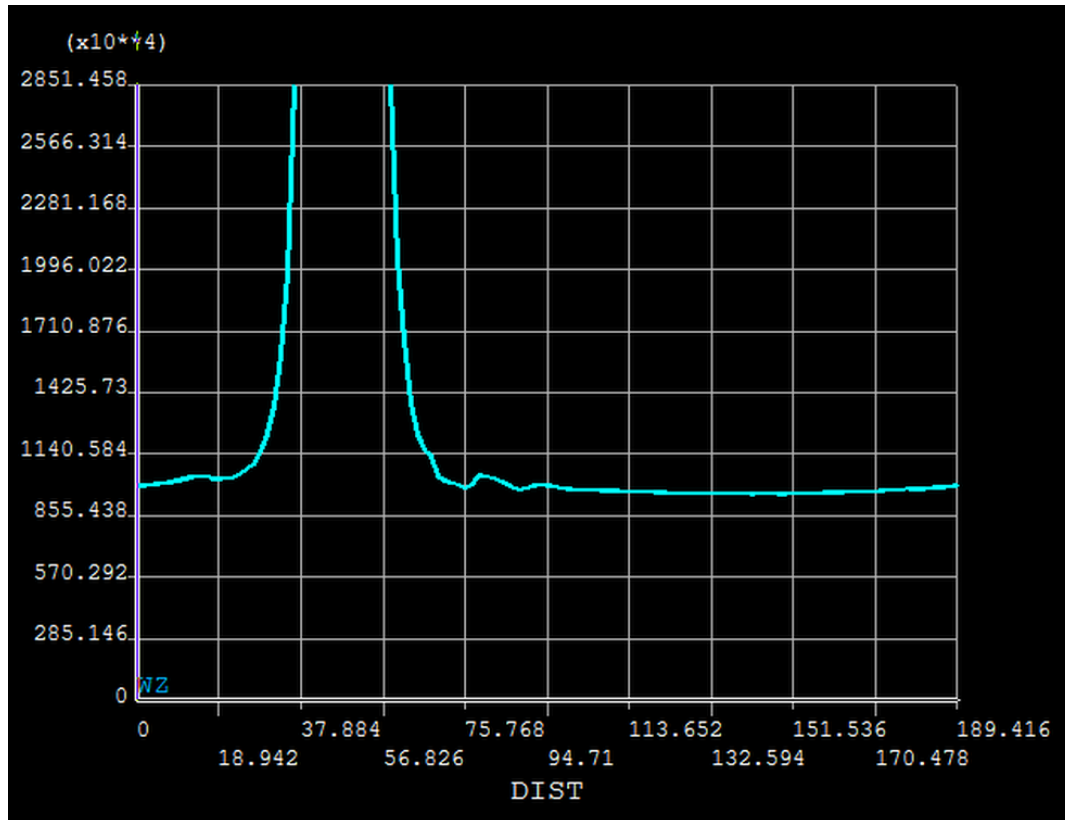


Figure 22: Plot of Stresses (Y axis) vs distance along a circumferential path (X axis) for 20mm hole

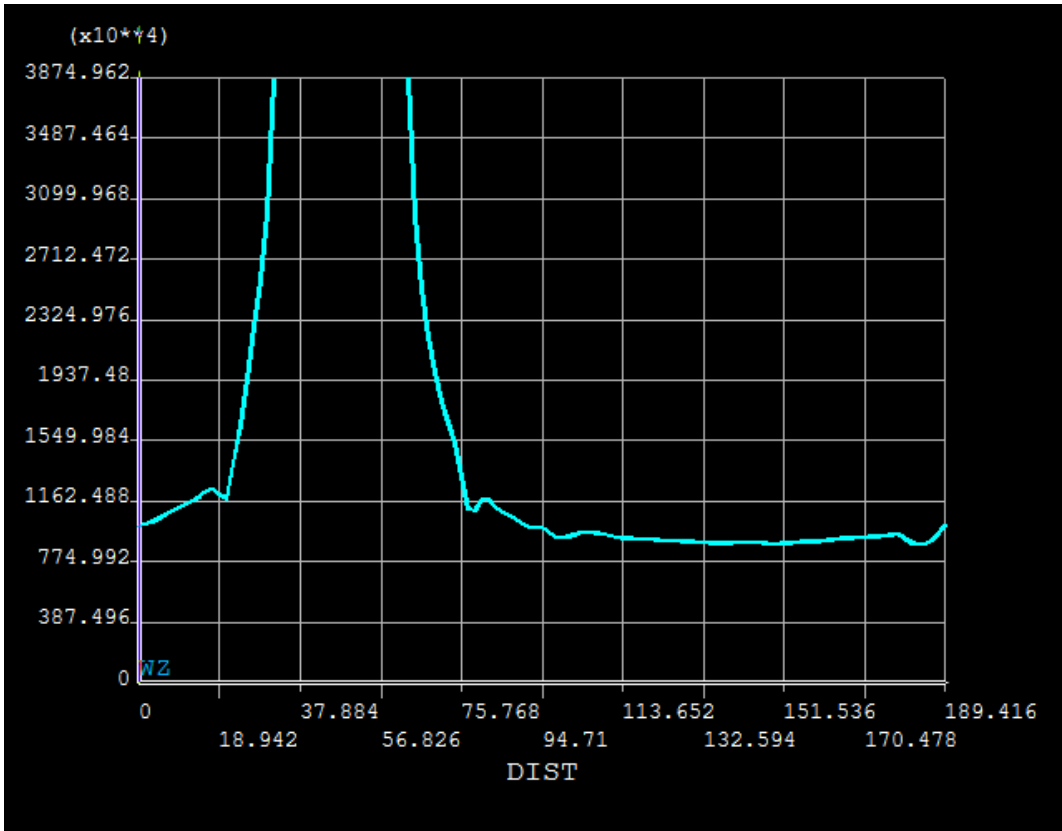


Figure 23: Plot of Stresses (Y axis) vs distance along a circumferential path (X axis) for 30mm hole

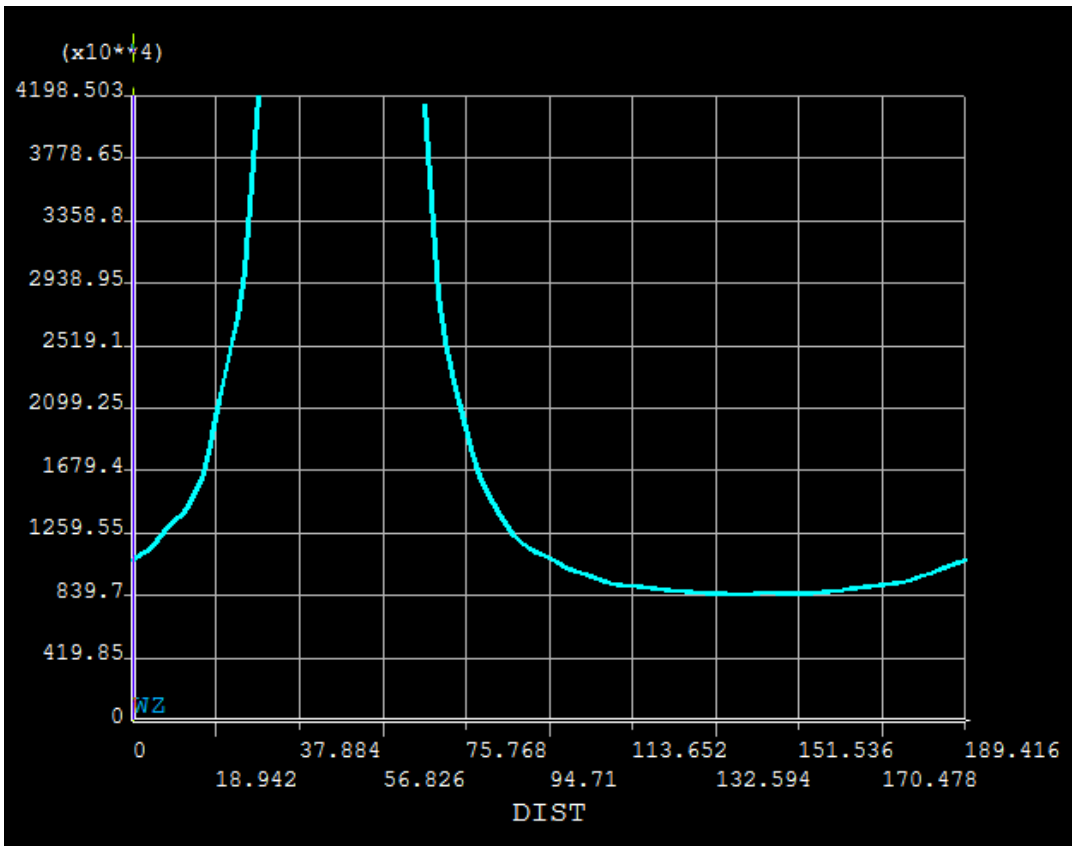


Figure 24: Plot of Stresses (Y axis) vs distance along a circumferential path (X axis) for 35mm hole

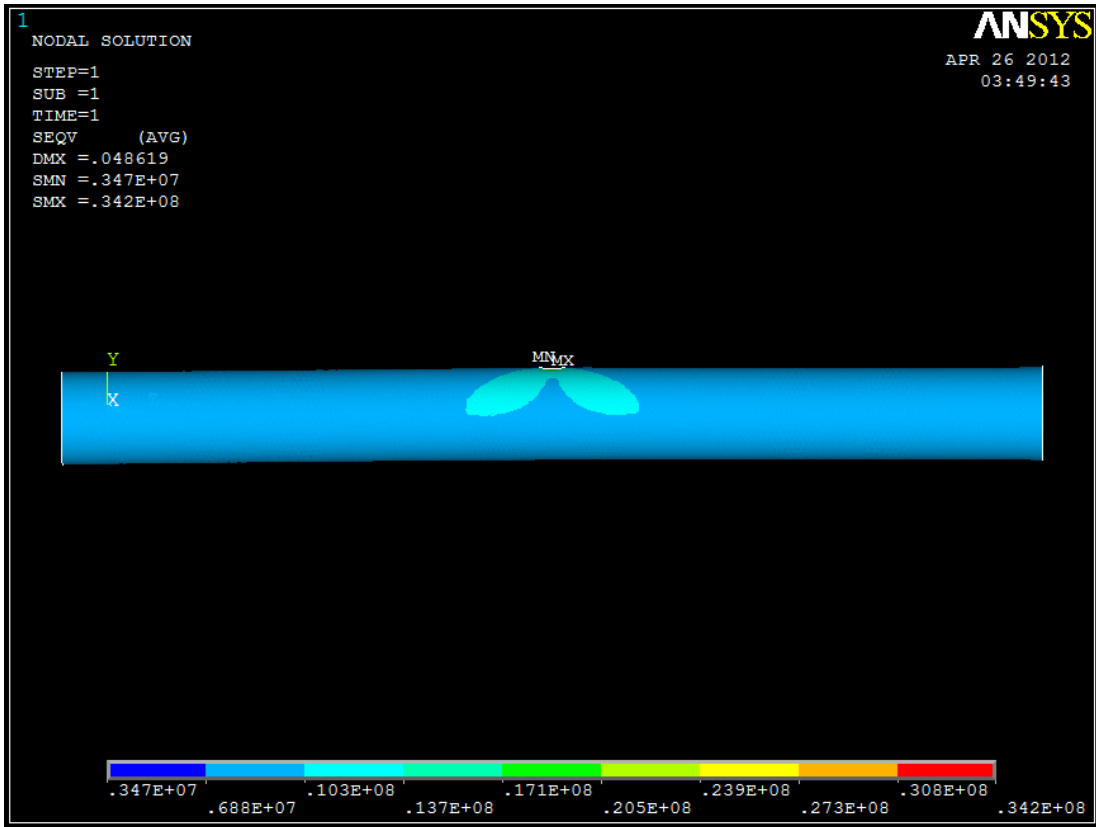


Figure 25: Distribution of stresses near the hole (side view)

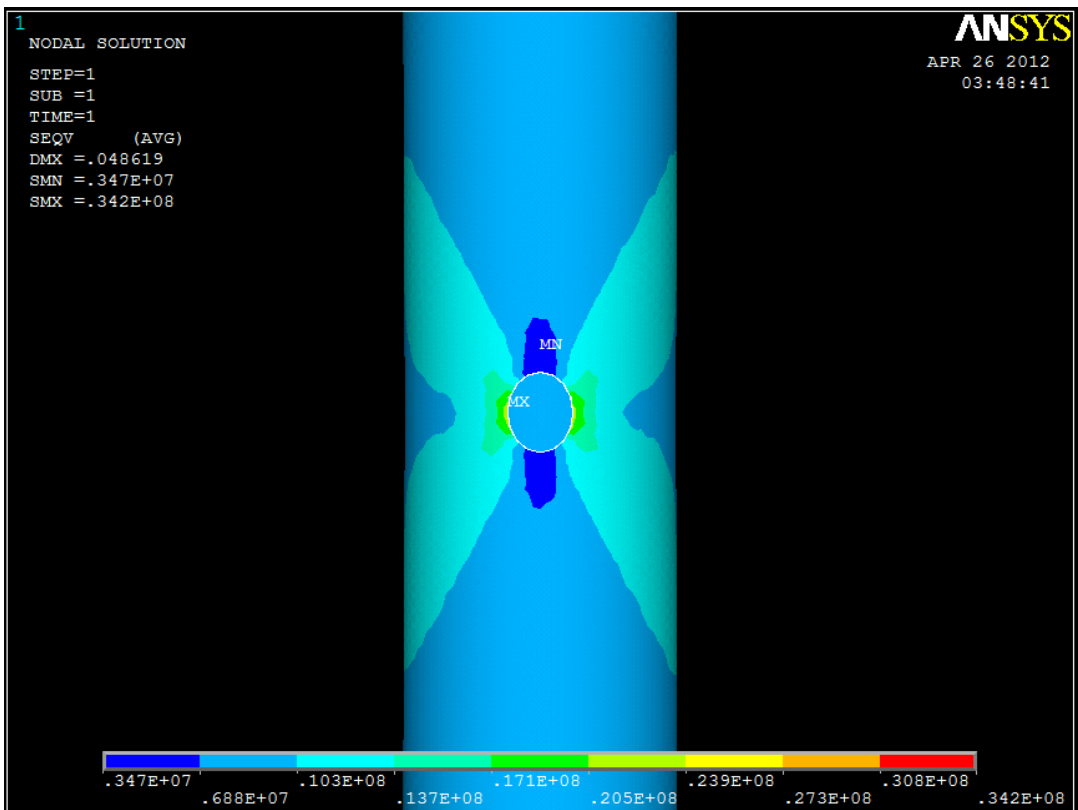
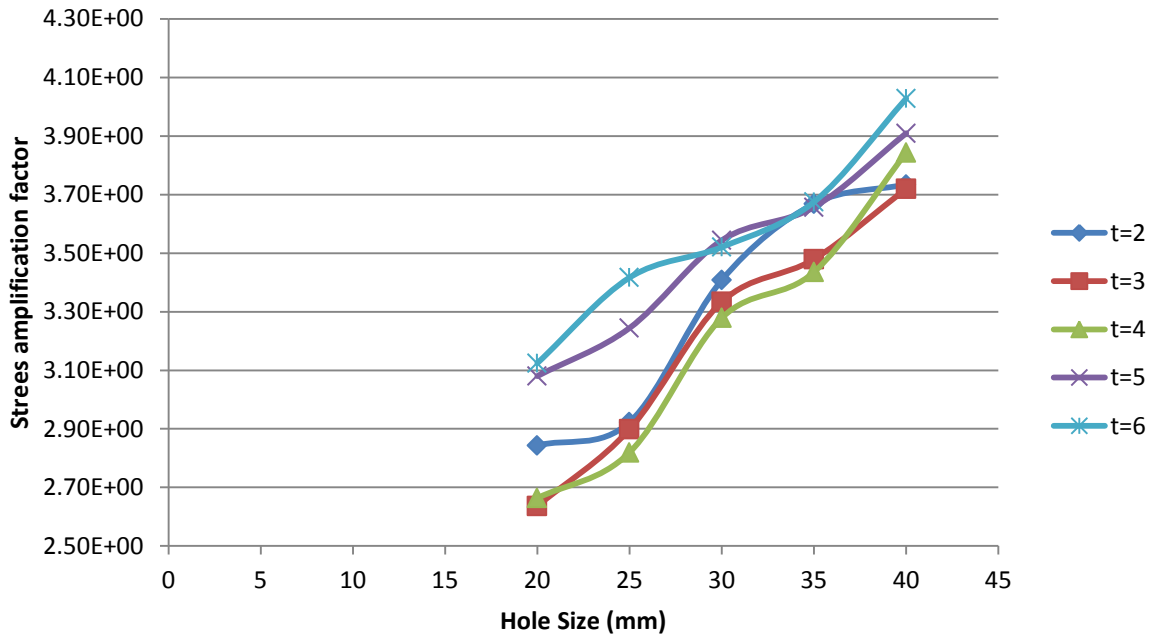
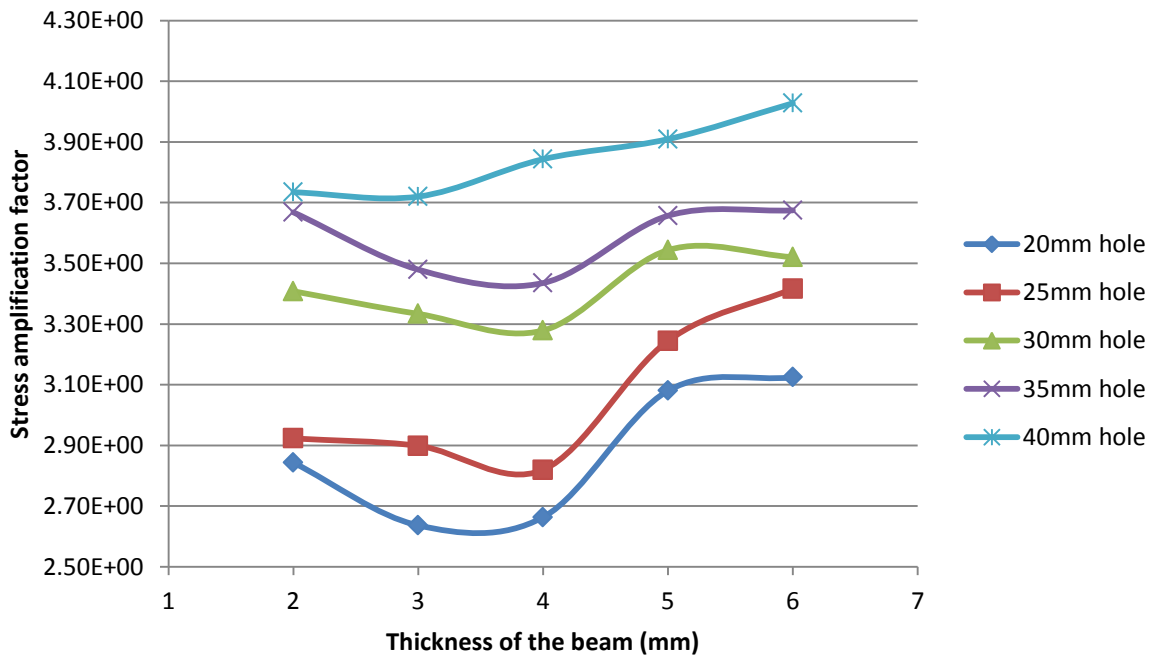


Figure 26: Distribution of stresses near the hole (enlarged top view)

Variation of amplification factor with hole size



Variation of amplification factor with beam thickness



3.4.1 Inference

The stress contours near the hole are similar to that predicted intuitively. A concentration of stress very close to the hole and the symmetricity of this distribution is expected. The increase in the amplification factor with increase in hole size is as expected. The role thickness plays is not very obvious from the plots. This is expected to be because of the amplification factor being a very complex function of thickness, hole size and outer diameter. It had been noticed from the simulations that the amount of force applied or the position of the hole did not make much of a difference to the amplification factor.

The main goal of this simulation was to check for an empirical relationship of the amplification factor with thickness of the beam, outer diameter and the hole size. This was not established since the relationship was not very obvious and is believed to be very complex functions of these parameters.

4. CONCLUSION

The stress/deflection patterns obtained by using TCE and our model are comparable; hence the our model of the antenna structure can be used for all further analysis without any further reference to the TCE model and analysis.

References

1. Books:
 - a. Finite element modeling. Schaum series
2. Papers:
 - a.